

UNCLASSIFIED

AD NUMBER
AD450756
NEW LIMITATION CHANGE
TO Approved for public release, distribution unlimited
FROM No foreign distribution.
AUTHORITY
ONR memo, 7 Jul 1965

THIS PAGE IS UNCLASSIFIED

UNCLASSIFIED

AD 4 5 0 7 5 6

DEFENSE DOCUMENTATION CENTER

FOR

SCIENTIFIC AND TECHNICAL INFORMATION

CAMERON STATION ALEXANDRIA, VIRGINIA



UNCLASSIFIED

NOTICE: When government or other drawings, specifications or other data are used for any purpose other than in connection with a definitely related government procurement operation, the U. S. Government thereby incurs no responsibility, nor any obligation whatsoever; and the fact that the Government may have formulated, furnished, or in any way supplied the said drawings, specifications, or other data is not to be regarded by implication or otherwise as in any manner licensing the holder or any other person or corporation, or conveying any rights or permission to manufacture, use or sell any patented invention that may in any way be related thereto.



450756

CATALOGED BY DDC

RADIO CORPORATION OF AMERICA, RCA LABORATORIES, PRINCETON, NEW JERSEY  
RCA 1110, INC.

# INTERACTIONS OF COHERENT OPTICAL RADIATION WITH SOLIDS

FINAL REPORT

by

R. BRAUNSTEIN and N. OCKMAN

Report Date: AUGUST 31, 1964

Contract No. NONR-4128(00)  
ARPA Order No. 306-62

Prepared for  
OFFICE OF NAVAL RESEARCH  
DEPARTMENT OF THE NAVY  
WASHINGTON 25, D. C.

4 5 0 7 5 6

1964-12-15 (revised) / 1964-12-15 (revised) / 1964-12-15 (revised)

Requests for additional copies by Agencies of the Department of Defense, their contractors, and other Government agencies should be directed to the:

DEFENSE DOCUMENTATION CENTER (DDC)  
CAMERON STATION  
ALEXANDRIA, VIRGINIA

Department of Defense contractors must be established for DDC services or have their "need-to-know" certified by the cognizant military agency of their project or contract.

**FINAL REPORT**

RADIO CORPORATION OF AMERICA, RCA LABORATORIES, PRINCETON, NEW JERSEY

**INTERACTIONS OF COHERENT OPTICAL  
RADIATION WITH SOLIDS**

*by*

**R. BRAUNSTEIN and N. OCKMAN**

*Report Date:* AUGUST 31, 1964

Contract No. NONR-4128(00)

ARPA Order No. 306-62

*Prepared for*

**OFFICE OF NAVAL RESEARCH  
DEPARTMENT OF THE NAVY  
WASHINGTON 25, D. C.**

Reproduction in whole or in part is permitted for any purpose of the United States Government. This research is part of Project DEFENDER under the joint sponsorship of the Advanced Research Projects Agency, the Office of Naval Research and the Department of Defense.

## PURPOSE

The aim of this research program was a study of the interactions of intense coherent optical radiation with solids. In this program, the experimental cross sections for double-photon absorption, harmonic generation, and frequency-mixing in semiconductors were to be compared with theory. The semiconductors of the group III-V and II-VI compounds were selected for study since reasonable predictions can be made regarding the strengths of these interactions utilizing the known band structure of these solids. The linear or single-photon interactions are reasonably well understood in these materials so as to provide the major band structure parameters which can be used to estimate higher-order intensity-dependent processes involving multiple-photon excitation via virtual states.

## ACKNOWLEDGMENTS

We would like to thank Mr. D. A. Kramer for having taken many of the measurements reported in the first three sections of this report, as well as having been responsible for the preparation of the samples used in the work described in those sections.

## SUMMARY

The study of double-photon absorption, harmonic generation, and frequency-mixing in semiconductors, and the frequency tuning of injection lasers by uniaxial stress are reported.

Observations were made of the two-photon excitation of an electron from the valence band to the conduction band in CdS ( $E_g = 2.5$  eV) using a pulsed ruby laser ( $\hbar\omega = 1.78$  eV). The radiative recombination emission from exciton and impurity levels subsequent to the simultaneous absorption of two quanta of  $\hbar\omega = 1.78$  eV was observed as a function of laser intensity and compared to the emission excited by single-quanta absorption for photons of  $\hbar\omega > E_g$ . It was found that the intensity of the recombination radiation is proportional to  $I_0^n$  for single-quanta excitation and  $I_0^{2n}$  for double-quanta excitation, where  $I_0$  is the excitation intensity and  $n$  is a constant which differs for different groups of emission lines. The observed cross section for double-quanta excitation is compared with theory utilizing the band parameters of CdS.

Calculations were also made of the cross sections for double-photon absorption in various substances. These results indicate that double-photon absorption can readily set an intrinsic upper limit to the power density that can be transmitted through a medium.

Substantial second-harmonic generation has been observed in the four III-V compound semiconductors InP, GaAs, AlSb and GaP. This radiation was generated at the exit faces of the single-crystal specimens by excitation using a Q-switched  $\text{Nd}^{3+}$  glass laser. The dependence of the harmonic intensity on both the polarization of the exciting and harmonic radiation as well as on the crystal orientations was studied and found to agree with the predicted behavior within experimental errors. In addition, the nonlinear susceptibilities,  $\chi_{14}$ , were determined and found to have the values of  $0.76 \times 10^{-6}$ ,  $1.07 \times 10^{-6}$ ,  $0.25 \times 10^{-6}$ , and  $0.18 \times 10^{-6}$  in electrostatic units for InP, GaAs, AlSb and GaP, respectively.

Mixing of the axial modes of both a ruby and a  $\text{Nd}^{3+}$  glass laser were observed in samples of Ge, GaAs, and Si which were subjected to an external dc bias field. The observed dependence of the intensity of the difference frequencies on the bias, excitation intensity, emitted frequencies and mobilities of these substances agrees with that expected for a photoconductive mixing mechanism.

The effect of uniaxial stress on the emission of GaAs diodes operating both in the lasing and nonlasing modes have been studied. It was demonstrated that the frequencies of these diodes can be readily tuned by as much as 0.5 percent by this method. Analysis of the frequency changes with stress for diodes prepared in different fashions indicates that different emission processes may be taking place. The modal structure of the laser frequencies and the output power from diodes fabricated by various techniques was also examined. These results, coupled with those obtained in our photomixing studies, indicates the feasibility of producing tunable power at much higher frequencies.

# TABLE OF CONTENTS

	<i>Page</i>
PURPOSE .....	iii
SUMMARY .....	v
LIST OF ILLUSTRATIONS .....	ix
<b>I. OPTICAL DOUBLE-PHOTON ABSORPTION IN SEMICONDUCTORS .....</b>	<b>1</b>
A. Introduction .....	1
B. Two-Band Model for Double-Photon Absorption .....	2
C. Transmission through a Nonlinear Medium .....	6
D. Discussion .....	8
<b>II. HARMONIC GENERATION IN FOUR III-V COMPOUNDS .....</b>	<b>11</b>
A. Introduction .....	11
B. Calculation of the Nonlinear Susceptibility .....	12
C. Experimental Techniques .....	14
1. Method of Measurement .....	14
2. Sample Preparation .....	15
D. Experimental Results .....	16
1. Polarization and Angular Dependence of Harmonic Generation .....	16
2. Determination of $\chi_{14}$ .....	20
E. Discussion .....	21
<b>III. FREQUENCY MIXING IN SEMICONDUCTORS .....</b>	<b>23</b>
A. Introduction .....	23
B. Experimental Arrangement .....	24
C. Experimental Results .....	26
D. Theory of Photoconductive Frequency Mixing .....	31
E. Discussion .....	32
<b>IV. FREQUENCY TUNING AND MIXING USING INJECTION LASERS .....</b>	<b>34</b>
A. Introduction .....	34
B. Frequency-Tuning by Uniaxial Stress .....	34
C. Properties of GaAs Lasers .....	39
D. Modal Structure of GaAs Emission .....	41
E. Mixing Experiments with Laser Diodes .....	43
REFERENCES .....	44

## TABLE OF CONTENTS (Continued)

	<i>Page</i>
<b>Appendices</b>	
I. OPTICAL DOUBLE-PHOTON ABSORPTION IN CdS .....	47
II. FREQUENCY TUNING OF GaAs LASER DIODE BY UNIAXIAL STRESS .....	59
III. EFFECT OF DOPING ON THE EMISSION PEAK AND ABSORPTION EDGE OF GaAs .....	63

## LIST OF ILLUSTRATIONS

<i>Figure</i>		<i>Page</i>
1	Schematic diagram of band structure model used to calculate double-photon absorption involving inter- and intra-band transitions .....	2
2	Transmission law for a medium with linear and quadratic losses simultaneously present .....	8
3	Experimental arrangement for measuring second harmonic emission .....	15
4	Intensity of harmonic generation in GaAs as a function of rotation about the normal to the (111) plane. $\psi$ is the angle between the vertical and the $\langle 001 \rangle$ direction for all of these figures. The polarizations of the incident and emitted radiation are specified in the figure; namely, the excitation is polarized horizontally and that of the emission vertically. The solid curve is the theoretical angular dependence; the circled points are the experimental results. The exit face (Ga side) was etched .....	17
5	Intensity of harmonic generation in GaAs as a function of rotation about the normal to the (110) plane. The difference between (a) and (b) lies in the different polarization of the excitation. The solid curves are the theoretical angular dependences; the circled points are the experimental points. The exit face was etched .....	18
6	Intensity of harmonic generation in GaAs as a function of rotation about the normal to the (110) plane. The difference between (a) and (b) is in the different polarization of the excitation. The solid curves are the theoretical angular dependences; the circled points are the experimental results. The exit face was polished but unetched .....	18
7	Intensity of harmonic generation in GaP as a function of rotation about the normal to the (111) plane. In (a) the exit face (Ga side) was etched for the circled points while the other points refer to the reverse etched exit face (P side). In (b) the circled points refer to a polished exit face while the other points refer to an etched exit face (Ga side). In addition, the two sets of points represent different polarizations as indicated. The solid curves are the theoretical angular dependences .....	19
8	(a) Intensity of harmonic generation in AlSb as a function of rotation about the normal to the (110) plane. The exit face was polished after being etched. (b) The same for InP as a function of rotation about the normal to the (111) plane. The circled points refer to an etched exit face while the others refer to one which was polished after being etched. The solid curves are the theoretical angular dependences .....	19
9	Schematic diagram for detecting microwave beat frequencies .....	25
10	Circuit diagram of pulse amplifier, time delay amplifier and relay for triggering laser and bias .....	26

## LIST OF ILLUSTRATIONS (Continued)

<i>Figure</i>		<i>Page</i>
11	Correlation between microwave and exciting laser signal. (a) The upper trace is the ruby laser and the lower trace is the 1.064-Gc signal from GaAs with sweep speed of 100 $\mu$ sec/cm. (b) The 1.537-Gc signal from Ge excited by a Nd laser; the upper trace shows the microwave signal while the lower trace displays the laser signal with sweep of 100 $\mu$ sec/cm. (c) Same experimental conditions as (b) but with sweep of 50 $\mu$ sec/cm .....	27
12	Microwave power output vs. bias and laser intensity for GaAs with ruby laser .....	28
13	Microwave power from Ge with Nd <sup>3+</sup> laser as a function of bias .....	29
14	Microwave power from Si with ruby laser vs. bias at 300°K and 78°K .....	30
15	Experimental arrangement for the compression measurements; the crystallographic orientation of the GaAs diodes used is indicated at the right .....	35
16	Recorder trace of the coherent emission line from a GaAs diode at three different stresses. The curves are displaced vertically for clarity. The linewidths are due to the unresolved modes. (Instrumental resolution $\sim 1\text{\AA}$ ) .....	36
17	Shift of the incoherent emission line from three typical GaAs diodes with uniaxial compression stress at 78°K. The indicated spread of the individual data points represents the variation of the results of all the measurements made at a given stress .....	37
18	Schematic diagram of uniaxial stress apparatus .....	39
19	Sketch of the far-field pattern of a GaAs diode with the simplest possible mode structures (diffraction effects) .....	40
20	Far-field pattern of GaAs laser diode .....	41
21	High resolution spectrum of GaAs laser .....	42
22	Diagram of mixing experiment using two GaAs lasers .....	43

# I. OPTICAL DOUBLE-PHOTON ABSORPTION IN SEMICONDUCTORS

## A. INTRODUCTION

In considering the probability for an N-photon process to take place in a given crystal for given input frequencies, the allowed process that involves the minimum number of photons will likely be dominant in the attenuation of the incident beam. Consequently, in the first phase of this program it was decided to study the double-photon absorption in semiconductors in the spectral region where single-photon absorption is forbidden. This process is of interest since it is an intrinsic absorption process which depends upon the incident intensity and is to be considered whenever a solid is irradiated with an intense light source of photons of energy greater than half the band gap.

An intrinsic semiconductor normally does not exhibit any optical absorption capable of producing electron-hole for photon energies less than the energy gap. This is true for the light intensities employed in conventional optical absorption experiments. However, for sufficiently high incident intensities of photons whose energy is less than the band gap, the multiple-photon excitation of a valence electron to the conduction band can take place and consequently, in principle, a perfectly transparent semiconductor does not exist!

In this section, we shall develop the theory for double-photon absorption in semiconductors and apply the results to calculate the double-quanta absorption cross section for the III-V compounds. The observed double-quanta absorption cross sections of CdS will also be compared with theory. The theory for the transmission through a medium where linear and quadratic absorption processes take place will be developed and it will be shown that double-photon absorption can set an intrinsic upper limit to the power density that can be transmitted through such media.

CdS was chosen for experimental study of the double-photon absorption. This selection was made primarily because the single-photon absorption process has been extensively studied in this substance, and it was therefore possible to compare double- and single-photon absorption on the same crystal. In addition, one can utilize the band structure parameters determined from single-photon absorption measurements to estimate the double-photon absorption coefficients. The theory developed for this process in CdS can also be readily applied to other II-VI and III-VI compounds. In addition, similar perturbation theory calculations for the three- and four-photon processes, i.e., second-harmonic generation and tripling can also readily be cast in a form that takes account of the band structure of these substances.

Observations were made of the two-photon excitation of an electron from the valence band to the conduction band in CdS ( $E_g = 2.5$  eV) using a pulsed ruby laser ( $\hbar\omega = 1.78$  eV). The radiative recombination emission from exciton and impurity levels subsequent to the simultaneous absorption of two-quanta of  $\hbar\omega = 1.78$  eV was observed as a function of laser intensity and

compared to the emission excited by single-quanta absorption for photons of  $\hbar\omega > E_g$ . It was found that the intensity of the recombination radiation is proportional to  $I_0^n$  for single-quanta excitation and  $I_0^{2n}$  for double-quanta excitation where  $I_0$  is the excitation intensity and  $n$  is a constant which differs for different groups of emission lines. The observed cross section for double-quanta excitation compared favorably with theory utilizing the band parameters of CdS; these results were published as an article in the Physical Review, a reprint of which is included in Appendix I.

Initially, the theory developed for the double-photon process in CdS utilized a three-band model for the band structure of this substance. However, the double-photon absorption cross section can easily be obtained using a two-band model employing a single valence and conduction band. We shall re-develop the double-photon calculation in this section utilizing the simpler band structure model, since it reveals simple generalizations regarding the underlying parameters which determine the double-quanta absorption cross section which apply to all the III-V compounds. This calculation enables one to set a lower bound to the double-photon absorption cross section while requiring a knowledge of very few band structure parameters. The theoretical development is essentially similar to that previously published<sup>1,2</sup> except that it utilizes an allowed intra-band optical transition for one of the virtual transitions.

## B. TWO-BAND MODEL FOR DOUBLE-PHOTON ABSORPTION

Consider a solid whose band structure consists of a valence band and a conduction band with extrema at  $k = 0$ ; a schematic diagram of this model is shown in Fig. 1. If two monochromatic photon beams of energies  $\hbar\omega_1$  and  $\hbar\omega_2$ , both less than the band gap, but whose sum is

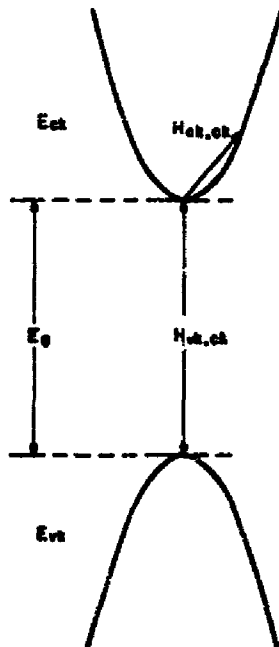


Fig. 1. Schematic diagram of band structure model used to calculate double-photon absorption involving inter- and intra-band transitions.

greater than the bandgap are incident upon the solid, the transition probability per unit time for an electron to be excited from an initial valence band state  $k$  to a final conduction band state  $k$  by the simultaneous absorption of two photons is given by

$$P_{vk,ck} = \frac{2\pi}{\hbar} \left| \frac{H_{vk,ck}H_{ck,ck}}{[E_{ck} + E_{vk} - \hbar\omega_1]} + \frac{H_{vk,ck}H_{ck,ck}}{[E_{ck} + E_{vk} - \hbar\omega_2]} \right|^2 \times \delta(E_g + E_{ck} + E_{vk} - \hbar\omega_1 - \hbar\omega_2) \quad (1)$$

where  $H_{vk,ck}$  is the optical matrix element which couples the valence band and the conduction band, and  $H_{ck,ck}$  is the intra-band optical matrix element coupling states within the conduction band.  $E_g$  is the separation of the valence and conduction band at  $k = 0$ ;  $E_{ck}$  and  $E_{vk}$  are the energies of the conduction and valence bands, respectively, as measured from their extrema. In this calculation, we have considered only one virtual state, while in fact it is usually necessary to sum over all possible intermediate states. The justification for this procedure is that a dominant contribution to the transition probability results from intermediate states which are closest to the final conduction band.

The absorption coefficient  $K_1$  for photon  $\hbar\omega_1$ , when  $\hbar\omega_1$  and  $\hbar\omega_2$  are simultaneously present, may be simply related to the number of  $\hbar\omega_1$  photons absorbed per unit time per unit volume and is given by

$$K_1 = \frac{-2n}{c} \frac{1}{N_1} \frac{\partial N_1}{\partial t} = \frac{2n}{cN_1} \sum_k P_{vk,ck} \quad (2)$$

where  $n$  is the index of refraction,  $c$  the velocity of light, and  $N_1$  the density of photons  $\hbar\omega_1$ . The factor of 2 is included in the absorption coefficient to account for the two electron spin orientations. We shall assume that there is very little spatial variation of the beam within the medium; that is, all absorption processes are small.

By combining Eqs. (1) and (2), the absorption coefficient is given by

$$K_1 = \frac{4\pi n}{cN_1\hbar} \int \frac{d^3k}{(2\pi)^3} \left[ \frac{H_{vk,ck}H_{ck,ck}}{(E_{ck} + E_{vk} - \hbar\omega_1)} + \frac{H_{vk,ck}H_{ck,ck}}{(E_{ck} + E_{vk} - \hbar\omega_2)} \right]^2 \times \delta(E_g + E_{ck} + E_{vk} - \hbar\omega_1 - \hbar\omega_2) \quad (3)$$

We have used the conventional optical matrix elements:<sup>3</sup>

$$H_{vk,ck} = \frac{e}{n_i m} \left( \frac{2\pi\hbar N_i}{\omega_i} \right)^{1/2} P_{vk,ck} \cdot \mathbf{a}$$

$$H_{ck,ck} = \frac{e}{n_i m} \left( \frac{2\pi\hbar N_i}{\omega_i} \right)^{1/2} P_{ck,ck} \cdot \mathbf{a}$$
(4)

where  $P_{vk,ck}$  and  $P_{ck,ck}$  are the appropriate momenta matrix elements,  $n_i$  is the refractive index at  $\omega_i$ , and  $\mathbf{a}$  represents a unit vector for the photon polarization.

To obtain explicit expressions for  $K_1$  for a given solid, it is necessary to have some knowledge of the momenta matrix elements as well as the  $\mathbf{k}$  dependence of  $E_{vk}$  and  $E_{ck}$ . If the transitions are allowed, that is, the coupling is between bands of opposite parity,  $|P_{vk,ck}|^2$  can be taken as a constant, and can be evaluated from the single-quanta absorption edge.  $P_{ck,ck}$  is a nonvanishing intra-band matrix element of zero order in  $\mathbf{k}$  which vanishes at an extrema and is equal to the group velocity times the free electron mass:<sup>4</sup>

$$P_{ck,ck} = mv = 1/\hbar \frac{\partial E_c}{\partial \mathbf{k}}$$
(5)

We shall assume that the energy bands are spherical and parabolic, and consequently are given by

$$E_{vk} = a_v \hbar^2 k^2 / 2m, \quad E_{ck} = a_c \hbar^2 k^2 / 2m$$
(6)

where the  $a$ 's are the inverse effective mass ratios. Substituting Eqs. (4), (5), and (6) into Eq. (3) and performing the integrations, we obtain the expression for the double-photon absorption coefficient:

$$K = \frac{(2)^{9/2} \pi N_2 a_c^2 |P_{vc}|^2 e^4}{c n_1 n_2^2 m^{3/2} (a_c + a_v)^{5/2}} \times [\hbar\omega_1 + \hbar\omega_2 - E_g]^{3/2} \times [1/\hbar\omega_1 + 1/\hbar\omega_2]^2$$
(7)

This expression is essentially similar to that previously obtained,<sup>1,2</sup> using the three-band model for the band structure, with the simplification that only one matrix element, the inter-band element remains to be specified, since we have performed the integration over the intra-band matrix element. It is seen that the characteristic features of the double-photon absorption process are still revealed; the absorption coefficient of photons  $\hbar\omega_1$  is a function of the density

$N_2$  of photons  $\hbar\omega_2$  simultaneously present in the solid; the intensity-dependent absorption edge increases as a power of photon energies with a threshold at  $\hbar\omega_1 + \hbar\omega_2 = E_g$ .

In order to evaluate Eq. (7) for a specific substance a knowledge of  $a_c$ ,  $a_v$ ,  $E_g$  and  $P_{vc}$  is necessary. It can be shown, using  $k \cdot p$  perturbation theory<sup>5</sup> to calculate the band structure of the zincblende semiconductors, that the valence and conduction band effective masses at  $k = 0$  and the single-quanta absorption edges can be accounted for by assuming that the inter-band momenta matrix element  $P_{vc}$  is constant<sup>6</sup> for all the III-V compounds and is given by  $|P_{vc}|^2 = 11.5 \text{ eV m}$ . It is instructive to re-express the absorption coefficient of Eq. (7) in terms of a non-linear absorption cross section normalized to unit flux per unit area; taking the above value for the square of the matrix element and assuming that  $\hbar\omega_1$  and  $\hbar\omega_2$  is approximately equal to  $E_g$  we obtain

$$\sigma_2 = \frac{3.6 \times 10^{-48} a_c^2}{n_1 n_2^2 (a_c + a_v)^{5/2}} \cdot \frac{1}{E_g^{5/2}} \text{ cm}^4 \text{ sec} \quad (8)$$

The conduction band effective masses for the III-V compounds are given from  $k \cdot p$  theory as

$$a_c = m/m_c = 1 + 2/3 |P_{vk,ck}|^2 \left( \frac{2}{E_g} + \frac{1}{E_g + \Lambda} \right) \quad (9)$$

where  $E_g$  is the band gap at  $k = 0$  and  $\Lambda$  is the spin-orbit splitting. The explicit values for the double-photon absorption cross sections from Eq. (8) for the III-V compounds can be obtained by assuming that the heavy-hole inverse effective mass ratio  $a_v = 1$  and using experimentally determined values<sup>6</sup> of  $a_c$ ,  $E_g$ , and  $\Lambda$  or the values of  $a_c$  calculated from Eq. (9). The values of  $\sigma_2$  for some representative compounds are shown in Table I.

TABLE I

	GaAs	InP	InAs	InSb
$E_g - \text{eV}$	1.53	1.34	0.45	0.25
$a_c -$	13.3	15.2	38.5	65.5
$\Delta -$	0.33	0.24	0.43	0.84
$\sigma_2 - \text{cm}^4 \text{sec}$	$2.8 \times 10^{-49}$	$3.7 \times 10^{-49}$	$4.0 \times 10^{-48}$	$1.4 \times 10^{-47}$

It is seen from Table I that the double-photon absorption cross sections increase as the band gap of the solid decreases. The characteristic feature that the absorption cross section increases as the band gap of the solid decreases is not limited to the case of a band-to-band transition in a semiconductor but comes from the frequency factors in the optical matrix elements in Eq. (4). This result is also obtained in the case of double-photon absorption between discrete levels; the nonlinear absorption cross section for such a process can be shown to be given by<sup>7</sup>

$$\sigma_2 = \frac{5.1 \times 10^{-48} f^2}{n^2 E_g^2 (\Delta E_g)} \text{ cm}^4 \text{ sec} \quad (10)$$

where  $n$  is the refractive index,  $\Delta E_g$  is the width of the real excited state at  $2E_g$ , and  $f$  is the  $f$ -number for the transition. In the derivation of Eqs. (8) and (10), it was explicitly assumed that the absorption occurs by a single intermediate state which allows coupling between the initial and final states. In fact, it is necessary to sum over all possible intermediate states. Consequently, these calculations represent a lower bound for the double-photon absorption cross sections.

We shall now compare the results of calculating the double-photon absorption cross-section for CdS using the present two-band model with the previous calculations using the three-band model.<sup>2</sup> The band parameters appropriate to CdS using a ruby laser are  $\alpha_c = 5$ ,  $\alpha_v = 0.2$ ,  $E_g = 2.5$  eV,  $\hbar\omega_1 = \hbar\omega_2 = 1.8$  eV and  $|P_{v_k, c_k}|^2 = 10.5$  eV m. The value of the momentum matrix element for CdS differs slightly from that of the III-V compounds; this value is in good agreement with experimental values of the effective masses of the II-VI compounds. The three-band model yields  $\sigma_2 = 3.3 \times 10^{-47}$  cm<sup>4</sup>sec for "allowed-allowed" transitions, while for the "allowed-forbidden" transitions  $\sigma_2 = 7 \times 10^{-48}$  cm<sup>4</sup>sec. Using the expression in Eq. (8) which was derived for a two-band model,  $\sigma_2 = 6 \times 10^{-49}$  cm<sup>4</sup>sec. The experimentally determined cross section for CdS is  $\sigma_2 \sim 10^{-48}$  cm<sup>4</sup>sec. Thus, virtual transitions involving intra-band matrix elements can make a reasonable contribution to the double-photon absorption cross section, and indeed it is necessary to sum over all inter- and intra-band transitions. Consequently, the double-photon absorption cross sections given by Eq. (8) represent a lower bound for this process.

### C. TRANSMISSION THROUGH A NONLINEAR MEDIUM

We shall now calculate an expression for the attenuation of a beam being propagated through a medium within which linear and quadratic loss processes can take place. In the steady state the transmitted flux through such a medium is given by the continuity equation

$$\nabla \cdot F = -\sigma_1 F N_1 - \sigma_2 F^2 N_2 \quad (11)$$

where  $\sigma_1$  is the linear absorption cross section in units of cm<sup>2</sup>,  $\sigma_2$  is the absorption cross section for a quadratic loss process in units of cm<sup>4</sup>sec, and  $N_1$  and  $N_2$  are the densities of centers responsible

for the linear and quadratic loss processes, respectively, and  $F$  is the flux per unit area in photons/cm<sup>2</sup>sec. We shall assume that  $N_1$  and  $N_2$  are independent of incident flux; i.e., the lifetime for recombination to the ground state is extremely short. For a plain parallel slab of thickness  $x$  and neglecting absorption losses, the transmission is obtained by integrating Eq. (11) we obtain

$$T = \frac{F}{F_0} = \frac{\sigma_1 N_1 x}{\sigma_1 N_1 x \exp[\sigma_1 N_1 x] + \sigma_2 N_2 x F_0 \exp[-\sigma_1 N_1 x] - \sigma_2 N_2 x F_0} \quad (12)$$

where  $F$  and  $F_0$  is the transmitted and incident flux in photons/cm<sup>2</sup>sec. We see that for high incident intensities, the transmission ultimately saturates. If the linear absorption is large or the incident flux is small, i.e.,

$$\begin{aligned} \sigma_1 N_1 x &\gg \sigma_2 N_2 x F_0 \\ T &= \exp[-\sigma_1 N_1 x] \end{aligned} \quad (13)$$

we obtain the conventional Lambert's law; that is, the output is proportional to the input. However, if the flux is high

$$\begin{aligned} \sigma_2 N_2 x F_0 &\gg \sigma_1 N_1 x \\ T &= 1 / 1 + \sigma_2 N_2 x F_0 \end{aligned} \quad (14)$$

the output is a nonlinear function of input; if  $\sigma_2 N_2 x F_0 > 1$  the transmission will decrease as a function of incident intensity.

Figure 2 shows a plot of the absorption  $A = 1 - T$  for a medium having linear and quadratic loss processes simultaneously present. When  $\sigma_2 N_2 x F_0 > 1$ , the quadratic loss becomes the dominant absorption process, and in fact the medium becomes opaque. Similar expressions can be readily derived for spherical and cylindrical geometries with results similar to Eq. (12) except for geometric factors; in such geometries, the transmission of the medium will also saturate as a function of incident flux. These results show that there is an intrinsic upper limit to the flux density which can be transmitted through a medium that has a nonlinear absorption process taking place. It should be further noted that it is only the linear absorption process that yields an exponential fall-off of intensity with distance and is independent of intensity, while the quadratic and higher order processes will fall-off inversely proportional to the distance and intensity.

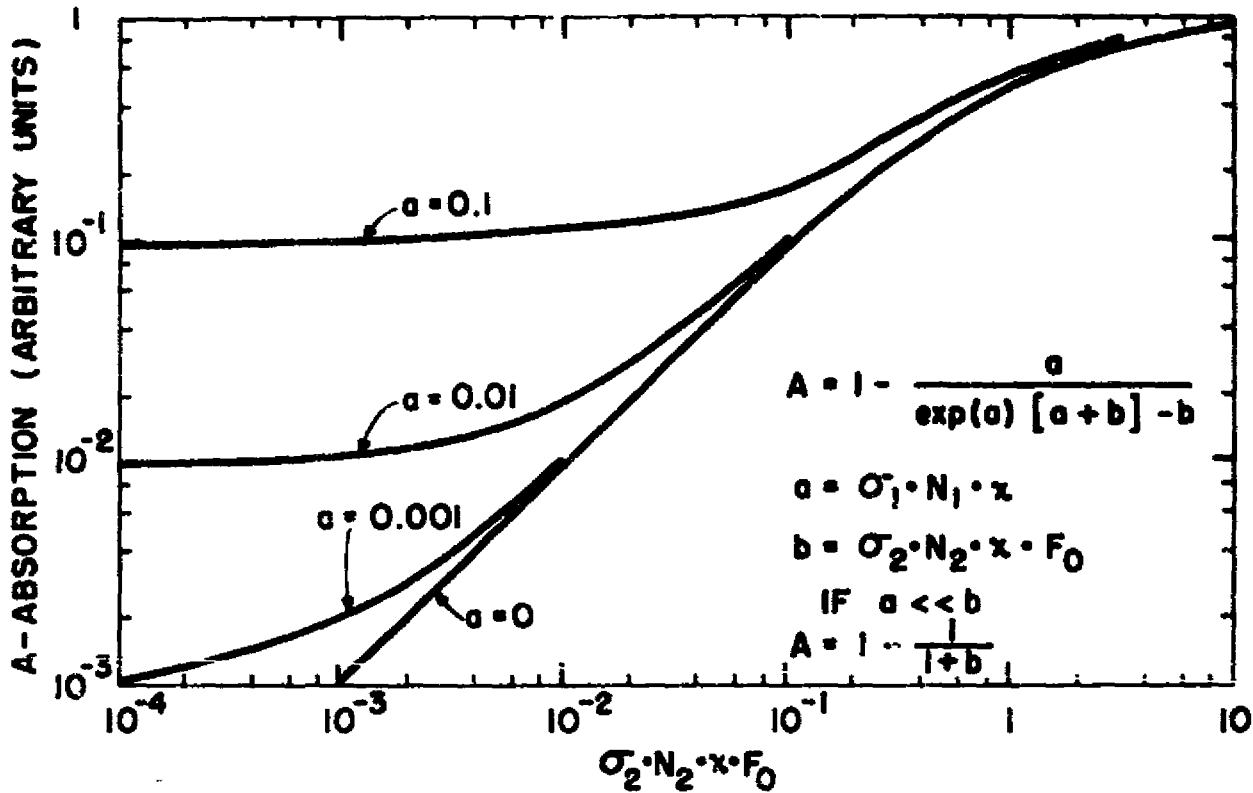


Fig. 2. Transmission law for a medium with linear and quadratic losses simultaneously present.

#### D. DISCUSSION

Although the double-photon absorption cross sections appear to be relatively small, since the absorption coefficient for this process depends upon the incident intensity, at high flux densities this process can constitute a major dissipative mechanism when operative.

It is of interest to consider the possible effects of double-quanta transitions on the power output of present injection lasers and in particular that of gallium arsenide. Although the power output presently available from such devices is relatively small, compared with that of optically pumped lasers, injection lasers are relatively small-area devices so that the flux per unit area is still quite high at the emitting junctions. Furthermore, the emitting frequencies lie slightly below the band gap satisfying the threshold conditions for double-photon absorption given in Eq. (7). Power densities of the order of  $10^7$  watts/cm<sup>2</sup> can be realized for conventional diodes. If one considers a diode 0.1 cm long with the above-mentioned power density and one employs the lower-bound, double-photon absorption cross section given in Table I for gallium arsenide, one obtains

$$\sigma_2 N_2 x F_0 = (3 \times 10^{-49}) \times (10^{22}) \times (10^{-1}) \times (10^{26}) = 3 \times 10^{-2} \quad (15)$$

From Eq. (12) and Fig. 2, we see that under these conditions the double-photon absorption can begin to make a contribution to the loss process within the structure. Even if an electron-hole

pair created by double-photon absorption subsequently recombined and re-emitted a photon, the double-photon absorption process would still set an intrinsic upper limit to the output power since two quanta will be annihilated to produce one subsequently re-emitted quantum.

If a focussed high-power laser is incident upon an ostensibly transparent substance such as calcium fluoride or another optical quality material, it is usually found that most substances tend to be punctured at power levels of approximately  $10^9$  watts/cm<sup>2</sup>. When one normally examines these materials by measuring the optical attenuation at low powers, it is usually found that such materials do not exhibit any absorption to account for the dissipated power necessary to destroy such material. Despite the fact that the band gap of these materials may be far greater than twice the incident photon energy so that a double-quanta process is not allowed between bands, it may be possible to have multiple-quanta processes taking place between impurity levels. If one considers as a typical example the case of optical-quality calcium fluoride one finds that one can have a distribution of impurity levels at concentrations of  $10^{18}$ /cm<sup>3</sup> due to various rare-earth impurities. A reasonable estimate of the double-photon absorption cross section for the ruby line at  $\hbar\omega_1 = 1.8$  eV can be made by superimposing the energy levels of the various impurities and using appropriate averages of the oscillator strengths and half widths for excited states at twice the laser frequency; the resulting cross section  $\sigma_2$  is  $10^{-49}$  cm<sup>4</sup>sec. For an incident beam of  $10^9$  watts/cm<sup>2</sup> and a 1-cm-thick slab

$$\sigma_2 N_2 \times F_0 \simeq (10^{-49}) \cdot (10^{18}) \cdot (1) \cdot (10^{28}) \sim 10^{-3} \quad (16)$$

Linear absorption due to scattering from optical imperfections or residual impurities normally yield values of  $\sigma_1 N_1 \times < 10^{-3}$  for optical quality calcium fluoride. Consequently, the normal linear scattering processes cannot account for the dissipation, while the double-quanta absorption due to impurities can be responsible for a reasonable amount of power absorbed from an incident beam.

In calculating the propagation of a laser beam through a gaseous atmosphere one normally utilizes the linear absorption coefficient of the appropriate optical window to determine the losses. However, if care is not taken so that no states exist at twice the laser frequency to which double-quanta absorption can take place, there is an intrinsic limit to the power that can be transmitted through such an atmosphere. Consider the case of a laser beam of photons of energy  $\hbar\omega \sim 3.1$  eV and a flux density of  $10^9$  watts/cm<sup>2</sup> propagated through a kilometer path length of O<sub>2</sub> at atmospheric pressure. For such a beam, double-photon absorption can take place via the Schumann-Runge bands. From the observed half-widths and oscillator strengths of these bands, the cross section  $\sigma_2$  can be estimated to be on the order of  $10^{-50}$  cm<sup>4</sup>sec; consequently

$$\sigma_2 N_2 \times F_0 \sim (10^{-50}) \cdot (10^{18}) \cdot (10^5) \cdot (10^{28}) \sim 10 \quad (17)$$

We see from Eq. (12) and Fig. 2 that the transmission of such a beam will saturate. Similar considerations will apply whenever one uses any optical window in an atmosphere where there is a state available at twice the frequency of the window so the double-photon absorption can take place.

In general, when evaluating the optical transmission of a material by observing experimentally the transmission of an optical beam at low intensities, it is dangerous to infer from these measurements, the loss mechanisms at high flux densities. As can be seen from Fig. 2, at low intensities the absorption can be independent of incident intensity, but if there is any quadratic loss process allowed, these could easily make overwhelming contributions to the absorption at high flux densities.

The above considerations of double-photon absorption also indicate that one can consider utilizing such a process for making extremely fast power limiters or optical shutters. Since the opacity of a material in which double-photon absorption can take place is dependent upon the flux density, some measure of control of the operating point of the limits is possible by placing such material at the appropriate point of an optical chain. Because of the intrinsically fast nature of the process, the time of response may not be limited by thermal lag or population relaxation times which prevail when single-quanta processes are used to perform such optical shuttering. For a broad-band device, one can utilize the band-to-band transitions in semiconductors or insulators if the  $\hbar\omega$  of the laser beam is greater than  $E_g/2$ . The estimated cross sections for most materials can be readily obtained from Eq. (8). In the case of discrete transitions, given by Eq. (10), if the half-width of a state at twice the laser frequency is very narrow, the cross sections of double-photon absorption can be quite high.

As we have seen from this work and the results reported in Appendix I, the calculated and observed double-photon absorption cross sections of CdS agree within an order of magnitude with theory, indicating that one can readily understand this process in terms of the band structure of a solid. The theory we have developed in this section, generalized to apply to the case of the III-V and II-VI compounds essentially sets a lower bound for the cross sections for double-photon absorption in these substances. These considerations indicate that it should be experimentally feasible to measure quite accurately the double-photon absorption cross sections in AlSb, GaAs, GaP, InP, and Si using a  $\text{Nd}^{3+}$  laser with  $\lambda = 1.06$  microns. Since injection lasers have been made from a number of semiconductors and alloys, the direct measurement of the nonlinear absorption in these substances would be of particular importance in ascertaining the intrinsic upper limit to the power output obtainable from such devices.

## II. HARMONIC GENERATION IN FOUR III-V COMPOUNDS

### A. INTRODUCTION

The investigation described in this section grew out of our success in obtaining reasonable agreement between the calculated and observed cross section for double-photon absorption in  $\text{CdS}^2$  which was discussed in the previous section. This result for  $\text{CdS}$  indicated to us that we might expect to find good correlation between theory and experiment for other nonlinear interactions of coherent radiation with semiconductors whose band structure is well characterized. The III-V semiconductor compounds comprise a group of materials whose band structure and related parameters are well known. Consequently, they are amenable to the calculation of cross sections for various nonlinear processes. In addition, these compounds lack a center of inversion and therefore, in principle, are capable of generating second harmonics of exciting frequencies which have sufficiently high intensities.<sup>8</sup> By comparing the measured harmonic cross sections  $\sigma_{2\omega}$  or as was done in our work, the nonlinear susceptibilities  $\chi_{14}$  (proportional to  $\sigma_{2\omega}^{1/2}$ ) of several III-V compounds having different band structure parameters, we sought to identify the pertinent parameters.

In this study we observed the second harmonic of a  $\text{Nd}^{3+}$  laser generated at  $5300 \text{ \AA}$  (2.34 eV) in single crystals of  $\text{InP}$ ,  $\text{GaAs}$ ,  $\text{AlSb}$ , and  $\text{GaP}$ . Our work on  $\text{InP}$  and  $\text{AlSb}$  is the first reported on these materials. Since the band gaps of these compounds range from 1.24 eV to 2.24 eV while the energy of the exciting photons was 1.17 eV, we were dealing with the case where the second harmonic was completely absorbed within a fraction of a wavelength after generation, while the exciting radiation suffered negligible attenuation. The emitted harmonic can be observed either in reflection or transmission. In the former, the harmonic is generated at the incident surface and is emitted as a reflected beam. In the latter the only harmonic radiation leaving the material is generated at the exit face since that produced in the bulk is completely absorbed. We employed the transmission method.

Shortly after we commenced this part of the program, Ducuing and Bloembergen<sup>9</sup> reported the first observation of harmonic generation in III-V compounds. They detected the emission of twice the ruby laser frequency in  $\text{GaAs}$  and  $\text{InSb}$  in reflection. They had to employ the reflection method since these materials are opaque to the exciting radiation. This was followed by the observation by Garfinkel and Engeler<sup>10</sup> of harmonics of several modes of the  $\text{GaAs}$  injection laser in  $\text{GaAs}$ . More recently, Bloembergen, Chang, Ducuing, and Lallemand<sup>11</sup> have reported the observation of reflected harmonics of both the ruby and neodymium lasers in  $\text{InSb}$ ,  $\text{InAs}$ ,  $\text{GaSb}$ , and  $\text{GaAs}$ . For the latter, they have also observed the emission in transmission for the neodymium excitation. Soref and Moos<sup>12</sup> have just published a very comprehensive study on harmonic generation in II-VI semiconductor alloy systems as well as in  $\text{GaAs}$  and  $\text{GaP}$  in the III-V category under present consideration.

An examination of the nonlinear susceptibilities of the seven III-V compounds studied so far shows that the absolute value for  $\chi_{14}$  for  $\text{Nd}^{3+}$  excitation lies between  $0.2 \times 10^{-6}$  esu and  $1.2 \times 10^{-6}$  esu. This compares with a value of  $3 \times 10^{-9}$  esu for KDP which is about the strongest harmonic emitter among ionic crystals. This 150- to 400-fold increase in  $\chi$  has been shown to be due mainly to the resonance between the harmonic and the conduction bands.<sup>12,13</sup> In the case of ionic crystals this does not occur for excitation by frequencies as low as those produced by the  $\text{Nd}^{3+}$  and ruby lasers.

This section on harmonic generation is divided into four parts: Section B is concerned with developing the equations that will be needed to calculate the nonlinear susceptibilities from the experimental data. In Section C we discuss the experimental methods used both in making the intensity measurements and preparing the samples. The intensity measurements as well as their dependence on the orientations of the polarization direction of the radiation with respect to crystallographic axes are presented in Section D. In Section D we also give the calculated values of  $\chi_{14}$ . Finally, in Section E we briefly discuss the consequences of our results.

## B. CALCULATION OF THE NONLINEAR SUSCEPTIBILITY

The problem which confronts us is the calculation of the harmonic power radiated by a parallel slab of nonlinear material upon which is incident an intense beam of coherent light. This problem was solved by Bloembergen and Pershan,<sup>14</sup> and the result can be obtained from Eq. (6.8) of their paper. Using Soref's simplification of this equation one finds that the square of the radiated harmonic field is given by

$$|E_{2\omega}|^2 = \frac{|4\pi P|^2 F}{(\epsilon'_{2\omega} - \epsilon'_\omega)^2 + (\epsilon''_{2\omega})^2} \quad (18)$$

where  $\epsilon'_{2\omega}$ ,  $\epsilon'_\omega$  are the real parts of the complex dielectric constant at frequencies  $2\omega$  and  $\omega$ , respectively.

$\epsilon''_{2\omega}$  is the imaginary part at frequency  $2\omega$ .

$P$  is the nonlinear polarization vector and for the  $Td(\bar{4}3m)$  symmetry of the III-V's is given by

$$P_i = \chi_{14} E_j E_k \quad (i,j,k \text{ refer to the crystallographic coordinate axes})$$

$F$  is a function of the complex dielectric constants or indices of refraction. In the case of a parallel slab in which the nonuniformity of the thickness is considerably larger than a wavelength (case in our experiment),  $F$  is given by

$$F = \frac{(n_{2\omega} + n_\omega)^2 + (k_{2\omega})^2}{(n_{2\omega} + 1)^2 + (k_{2\omega})^2} \quad (\text{For } k_{2\omega} = 0, F \text{ is different})$$

$n_{2\omega}$  and  $n_{\omega}$  are the real indices of refraction at  $2\omega$  and  $\omega$ , respectively; and  $k_{2\omega}$  is the extinction coefficient at  $2\omega$ . We can express  $(n_{2\omega})^2$ ,  $(n_{\omega})^2$  and  $(k_{2\omega})^2$  as functions of the complex dielectric constants as follows:

$$(n_{2\omega})^2 = \frac{\epsilon'_{2\omega}}{2} + \frac{\sqrt{(\epsilon'_{2\omega})^2 + (\epsilon''_{2\omega})^2}}{2}; \text{ similarly for } (n_{\omega})^2$$

$$(k_{2\omega})^2 = \frac{\epsilon''_{2\omega}}{2} + \frac{\sqrt{(\epsilon'_{2\omega})^2 + (\epsilon''_{2\omega})^2}}{2}$$

In our experiments, we excited our crystals with linearly polarized light and measured the polarized intensities of the harmonics. As shown in a later section, we can express the polarization as

$$P = K \chi_{14} G(\psi) (E_L)^2 \quad (19)$$

where  $K$  is a constant for given crystal and polarizer orientations.

$G(\psi)$  is a function of the angle which the crystal  $\langle 001 \rangle$  axis makes with a direction in space.

$E_L$  is the linearly polarized electric field of the laser inside the crystal.

Inserting this expression into Eq. (18) and converting the fields into power by means of Poynting's theorem<sup>15</sup> one obtains

$$W_{2\omega} = \left( \frac{8\pi}{CA} \right) \frac{64 \pi^2 K^2 (\chi_{14})^2 [G(\psi)]^2 (I_{\omega})^2 F}{(n_{\omega})^2 (1+n_{\omega})^4 (1+n_{\omega}^2)^2 [(\epsilon'_{2\omega} - \epsilon'_{\omega})^2 + (\epsilon''_{2\omega})^2]} \quad (20)$$

where  $W_{2\omega}$  is the harmonic power radiated from the slab.

$I_{\omega}$  is the laser power measured after traversal of the slab by the beam.

$A$  is the area of the beam

If one uses cgs units  $|\chi_{14}|$  will be expressed in esu.

Although Eq. (20) could be used to obtain  $\chi_{14}$ , it would require an absolute measurement of  $W_{2\omega}/(I_{\omega})^2$  which would require an accurate calibration of attenuating filters and photomultipliers. It is much simpler to compare the harmonic power of an unknown with a known generator. Since the  $\chi$  of KDP is known far more accurately than our experiments could measure any of our materials,<sup>16</sup> we used it as our reference substance.

Again utilizing the results for a parallel slab used in obtaining Eq. (18) we obtain for a nonuniform slab of KDP having (110) faces the following expression for the harmonic power

$$W_{2\omega} = \left(\frac{8\pi}{CA}\right) (1.14 \times 10^4) |X_{14}^K|^2 \left(\frac{I_{\omega}^K}{i_{\omega}}\right)^2 \quad (21)$$

This expression comes from the evaluation in Eq. (20) of the various factors for KDP. We used the following values for the indices,  $n_{\omega}^0 = 1.497$ ,  $n_{2\omega}^e = 1.471$ ,<sup>17</sup> since the orientation of the KDP was such that the laser beam entered as an ordinary ray producing an extraordinary harmonic ray.

To obtain the equation used in our work to calculate the nonlinear susceptibilities relative to KDP divide Eq. (20) by Eq. (21) and solve for  $|X_{14}|^2/|X_{14}^K|^2$ . The result is

$$\frac{|X_{14}|^2}{|X_{14}^K|^2} = \frac{W_{2\omega}}{W_{2\omega}^K} \left(\frac{I_{\omega}^K}{i_{\omega}}\right)^2 \mathcal{L} \quad (22)$$

where

$$\mathcal{L} = \frac{300(n_{\omega})^2 (1+n_{\omega})^4 (1+n_{\omega}^2)^{-2} [(\epsilon'_{2\omega} - \epsilon'_{\omega})^2 + (\epsilon''_{2\omega})^2]}{\pi^2 K^2 [G(\psi)]^2 F}$$

Hence, a measurement of the harmonic and monitor powers relative to a crystal of KDP enables one to determine the relative magnitude of the  $X_{14}$ 's.

## C. EXPERIMENTAL TECHNIQUES

### 1. Method of Measurement

The experimental setup is shown in Fig. 3. We used a Q-switched laser made by Lear Siegler, Inc., with a 2½-inch Nd<sup>3+</sup> glass rod. The Q-spoiler is a prism rotating at 60 cps. To prevent damage to our samples we operated the laser slightly above threshold. The emission consisted of a single pulse with a maximum power of about 10<sup>5</sup> watts and having a half-width of about 0.1 μsec. Following the laser were two filters designed to cut out the uv flashlamp emission. This was followed by a Glans air prism which polarized the laser excitation. The samples were mounted on a goniometer head to facilitate orientation. For AlSb we had to place the crystal in an air-tight cell containing Drierite to prevent moisture from attacking the surfaces. An 1/8-in. aperture was used in measuring relative intensities for determining  $X_{14}$ . It assured an equal area of emission for all of our samples. The glass beam-splitter directed a small fraction of the laser radiation into the monitoring 7102 photomultiplier. The Corning filters gave the necessary attenuation of about 10<sup>8</sup>. The 4-96 filter, Kodak attenuator and polaroid in front

of the 1P28 photomultiplier allowed only a polarized component of the harmonic into the photomultiplier. The signals were observed on a Tektronix 502 dual-beam oscilloscope which was triggered by the monitor signal.

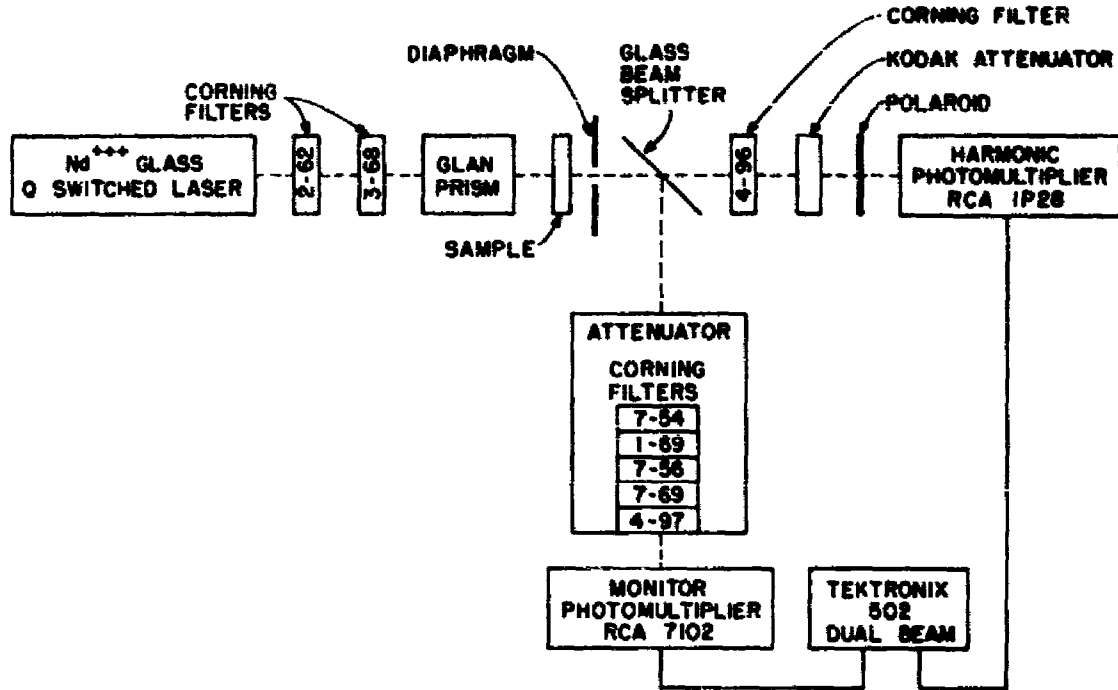


Fig. 3. Experimental arrangement for measuring second harmonic emission.

Several comments should be made here. Initially, we observed the harmonics by means of a spectrometer to ensure that we were seeing the desired radiation. However, we were able to obtain larger signals without the spectrometer and still adequately filter out unwanted emission from the laser and flashtube. Unfortunately, we had insufficient laser intensity to use the harmonic from a KDP crystal as a monitor. This would have been desirable since it has been shown<sup>18</sup> that the fluctuations of the harmonic emission follows a harmonic monitor much more closely than the direct laser intensity because of the fluctuations in the coherence properties of the laser in successive bursts of emission. This is one reason for the large fluctuations in our data which are presented in Section II-D.

## 2. Sample Preparation

The crystals of GaAs, InP, and GaP were grown at the RCA Laboratories and kindly furnished us. The AlSb sample was obtained from Battelle Memorial Institute. Of the RCA crystals, GaP was grown epitaxially, InP by the Bridgman method, and GaAs by the Czochralski process. Only the GaP crystal was doped (with sulfur) and had a carrier concentration between  $10^{17}$  and  $10^{18}$  per cc. The carrier concentrations in GaAs (111), GaAs (110), InP (111) and AlSb (110) were  $3.6 \times 10^{16}$ ,  $1.4 \times 10^{16}$ ,  $3.22 \times 10^{16}$  and  $2 \times 10^{17}$ , respectively. The crystal orientations were established by X-ray analysis.

Since the harmonics are generated within a fraction of a wavelength of the exit face, one might expect that their intensities are very sensitive to chemical surface treatments. In addition, one might expect that mechanical operations like polishing would produce lattice disorientations at the surface which would result in several crystallographic planes contributing simultaneously to the harmonic intensity. This would show up as a nonvanishing minimum in the orientational dependence of the harmonics. In the experiments, we encountered both of these effects.

We investigated the effect of various polishing etches on the harmonic intensity. For the intensity measurements used in determining  $\chi_{14}$ , we chose the surface treatment which gave both the maximum emission and a zero or almost zero emission at the sample orientations where it should vanish. Both faces of all samples were polished with fine corundum prior to etching. It was also beneficial to polish the faces irradiated by the laser after the samples were etched. The optimum etches were:

- InP            – HNO<sub>3</sub> + HCL (dull smooth side toward laser)
- GaAs(111) – aqua regia (rough As side toward laser)
- GaAs(110) – 6H<sub>2</sub>SO<sub>4</sub> + H<sub>2</sub>O<sub>2</sub> + H<sub>2</sub>O (both sides identical)
- AlSb           – best results with both faces polished and unetched
- GaP           – 3H<sub>2</sub>SO<sub>4</sub> + 6HNO<sub>3</sub> + HF + 10 drops of Br<sub>2</sub> (smooth P side toward laser)

## D. EXPERIMENTAL RESULTS

### I. Polarization and Angular Dependence of Harmonic Generation

To determine the nonlinear susceptibilities it was shown in Section II-B that we have to determine the function  $KG(\psi)$  which depends both on the crystallographic face and the polarization of the laser and the harmonic radiation. The reason that harmonic emission in these cubic crystals is anisotropic can be seen from the relation previously given; namely,  $P_i = \chi_{14} E_j E_k$ . Since the i, j, and k axes are fixed in the crystal we have to relate these directions to those outside the crystal determined by the polarization directions of the exciting and emitted radiations. The results of these trigonometric calculations for both the (111) and (110) crystallographic faces are presented in Table II for the orthogonal polarizations used in our experiment.

Figures 4 through 8 show both the functions from Table II and the corresponding experimental points for the four crystals studied. In cases where more than one measurement was made at one angle, the error bars were inserted to indicate the maximum deviation from the average. The largest deviations range from about  $\pm 25\%$  to  $\pm 60\%$  which is also the size of the largest discrepancies from the theoretical curves. In general, the deviations were considerably smaller. These curves show that the bulk crystallographic structure is preserved down to thicknesses of the order of 1000 Å. The harmonics vanish at the predicted angles except for the GaP crystal, thus indicating that the surface preserves the bulk crystal structure whether the surface was

etched or polished. This was not quite true for GaP for both surface treatments. We also found that polished crystals of GaAs behaved similar to GaP.

Since our results for the laser polarized horizontally and the analyzer vertical seemed to lie closest to the expected behavior, we chose these polarizations for making our quantitative relative intensity measurements for determining  $\chi_{1,4}$ . Since the maximum harmonic production for these polarizations occurs when  $\chi = 0$  for both the (111) and (110) faces we oriented our samples with their  $\langle 001 \rangle$  axes vertical for these measurements.

TABLE II  
 $KG(\psi)$  FROM EQ. (19) FOR TRANSMISSION AT NORMAL INCIDENCE

	(111) FACE	
	$E_L$ VERT.	$E_L$ HOR.
$P_{2\omega}$ vert.	$3/4 \sin^3 \theta \cos \psi (1-4 \sin^2 \psi)$	$3/4 \sin^3 \theta \cos \psi (1+4 \sin^2 \psi)$
$P_{2\omega}$ hor.	$3/4 \sin^3 \theta \sin \psi (3+4 \sin^2 \psi)$	$3/4 \sin^3 \theta \sin \psi (1-4 \cos^2 \psi)$
	(110) FACE	
	$E_L$ VERT.	$E_L$ HOR.
$P_{2\omega}$ vert.	$3/2 \sin^2 \psi \cos \psi$	$1/2 \cos \psi (1-3 \sin^2 \psi)$
$P_{2\omega}$ hor.	$1/2 \sin \psi (1-3 \cos^2 \psi)$	$3/2 \cos^2 \psi \sin \psi$

Where  $\theta = 54^\circ$   
 $\psi =$  angle between polarizer and  $\langle 001 \rangle$  axis

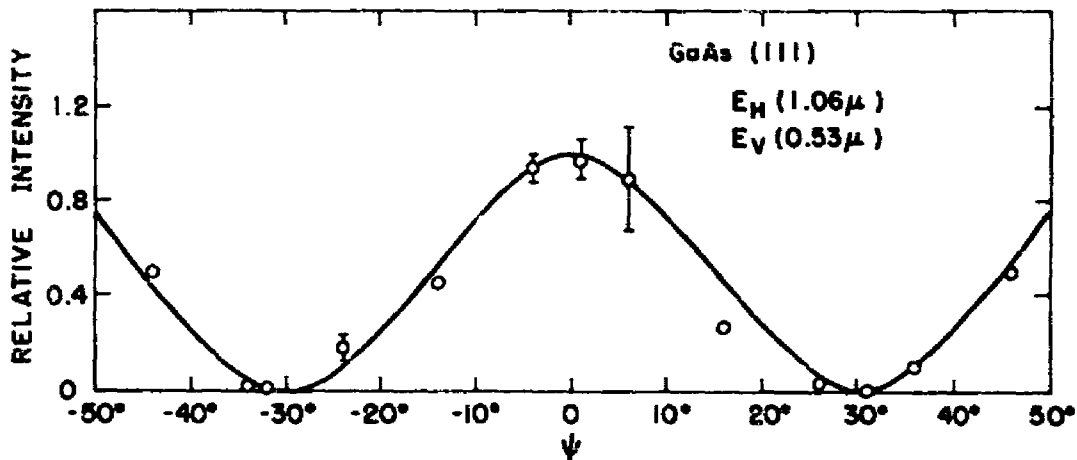


Fig. 4. Intensity of harmonic generation in GaAs as a function of rotation about the normal to the (111) plane.  $\psi$  is the angle between the vertical and the  $\langle 001 \rangle$  direction for all of these figures. The polarizations of the incident and emitted radiation are specified in the figure; namely, the excitation is polarized horizontally and that of the emission vertically. The solid curve is the theoretical angular dependence; the circled points are the experimental results. The exit face (Ga side) was etched.

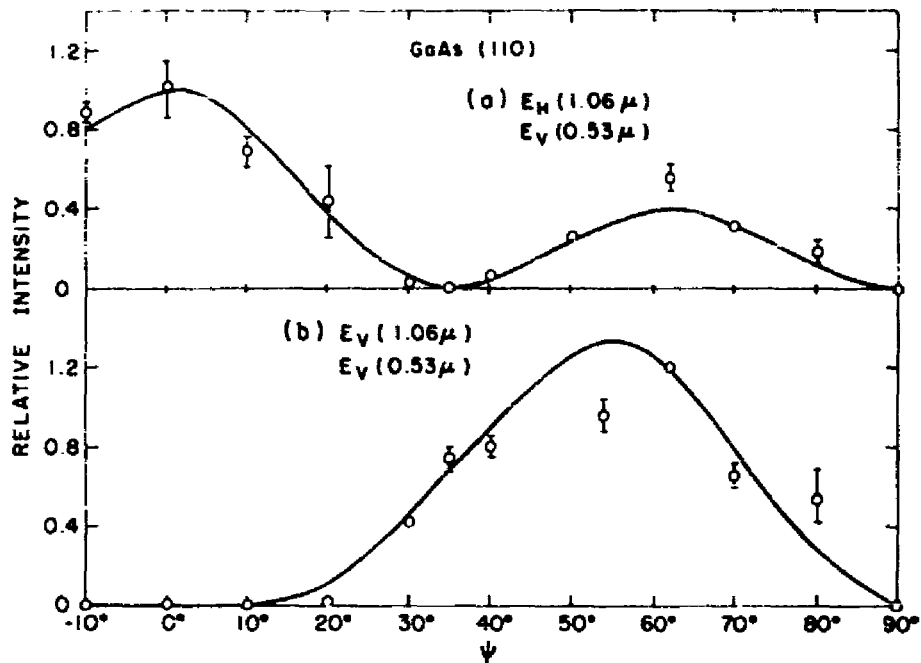


Fig. 5. Intensity of harmonic generation in GaAs as a function of rotation about the normal to the (110) plane. The difference between (a) and (b) lies in the different polarization of the excitation. The solid curves are the theoretical angular dependences; the circled points are the experimental points. The exit face was etched.

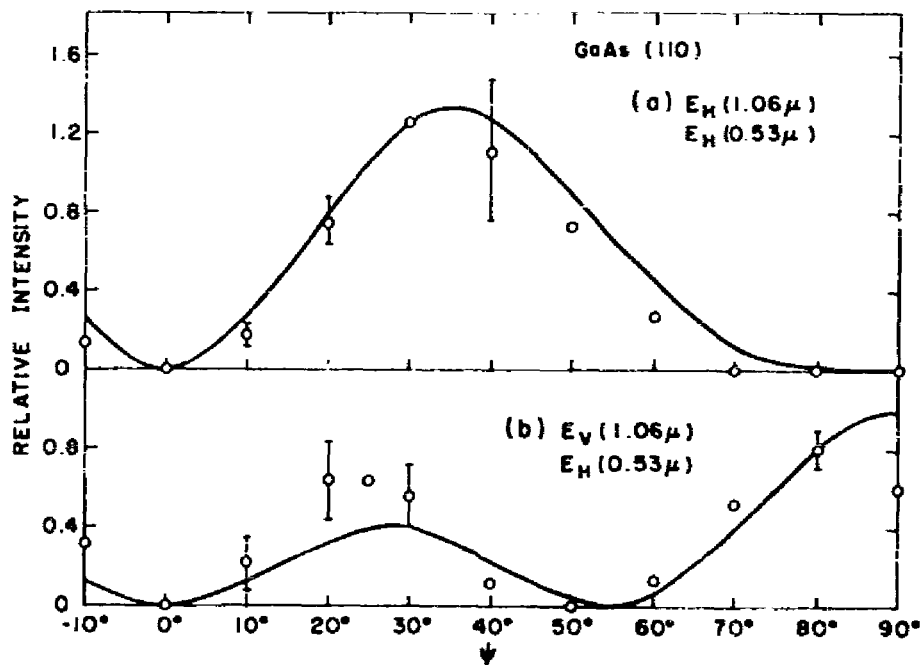


Fig. 6. Intensity of harmonic generation in GaAs as a function of rotation about the normal to the (110) plane. The difference between (a) and (b) is in the different polarization of the excitation. The solid curves are the theoretical angular dependences; the circled points are the experimental results. The exit face was polished but unetched.

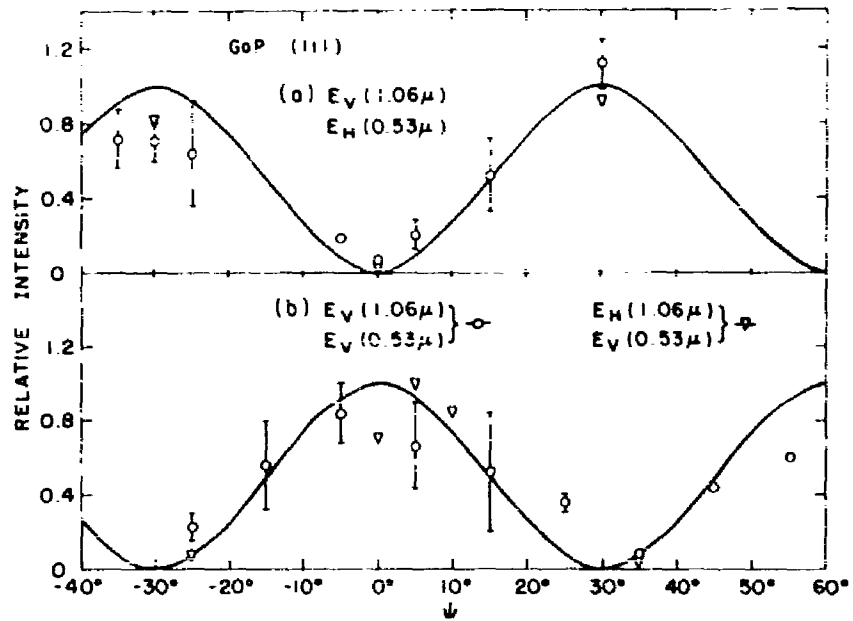


Fig. 7. Intensity of harmonic generation in GaP as a function of rotation about the normal to the (111) plane. In (a) the exit face (Ga side) was etched for the circled points while the other points refer to the reverse etched exit face (P side). In (b) the circled points refer to a polished exit face while the other points refer to an etched exit face (Ga side). In addition, the two sets of points represent different polarizations as indicated. The solid curves are the theoretical angular dependences.

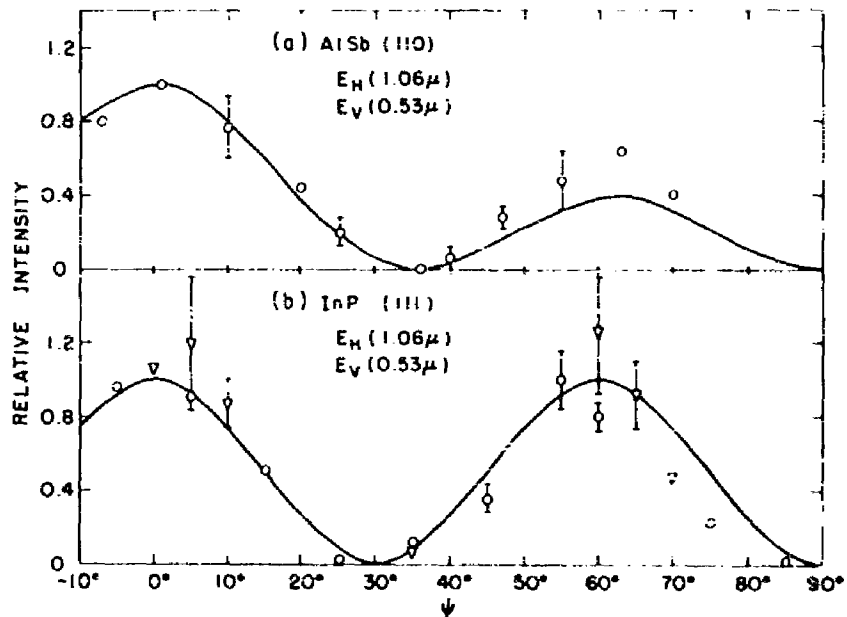


Fig. 8. (a) Intensity of harmonic generation in AlSb as a function of rotation about the normal to the (110) plane. The exit face was polished after being etched. (b) The same for InP as a function of rotation about the normal to the (111) plane. The circled points refer to an etched exit face while the others refer to one which was polished after being etched. The solid curves are the theoretical angular dependences.

## 2. Determination of $\chi_{14}$

To obtain the nonlinear susceptibilities we need to evaluate the function  $\mathcal{L}$  in Eq. (22) and then insert the intensities for both KDP and each of the compounds under consideration. The pertinent optical constants as well as the calculated function,  $\mathcal{L}$ , are given in Table III. Since the dielectric constants for GaAs and GaP were obtained from measuring off a small drawing we would place an uncertainty of about  $\pm 5\%$  on these values. The extrapolation procedure for InP and AlSb would increase this uncertainty to a possible  $\pm 10\%$ .

TABLE III  
OPTICAL CONSTANTS FOR THE III-V COMPOUNDS

	InP (111)	GaAs (111)	AlSb (110)	GaP (111)
$^*E_g$	1.26 eV	1.35 eV	1.60 eV	2.24 eV
$\epsilon'_{2\omega}$	17.9	**17.2	15.4	**10.6
$\epsilon'_{\omega}$	11.9	**11.7	10.9	** 9.0
$\epsilon''_{2\omega}$	3.2	** 2.8	2.1	** 0
$k_{2\omega}$	0.15	0.12	0.10	0
$n_{2\omega}$	4.24	4.16	3.87	3.25
$n_{\omega}$	3.44	3.41	3.30	3.00
$\mathcal{L}$	$1.8 \times 10^5$	$9.4 \times 10^4$	$3.5 \times 10^4$	$5.2 \times 10^3$

\* Ref. T. S. Moss, *Optical Properties of Semi-Conductors* (Acad. Press, 1959) p. 224.

\*\* Ref. H. R. Phillipp, H. Ehrenreich, *Phys. Rev.* **129**, 1550 (1963).

The values of the complex dielectric constants for InP and AlSb were obtained by linear extrapolation using the measured values for GaAs and GaP.

The measured intensities for both the monitored laser frequency and the harmonic, together with the calculated susceptibilities are displayed in Table IV. The corrected  $\chi_{14}$  values refer to a correction for scattering losses at the exit surfaces where the harmonics were generated. This correction, which is of approximate nature, is based on the observation that the monitored intensities for our samples were smaller than they should have been if the only loss of the laser beam traversing a sample was due to reflection at both surfaces. We assumed that there were no losses in the bulk,<sup>19</sup> that the monitor losses were equal at both surfaces, and that the losses were the same at the harmonic frequency as at the laser frequency. Consequently, we were able to calculate the losses at the exit surfaces and have inserted these corrections in

the table. We list both values of  $\chi_{14}$  due to the uncertain nature of this correction. The larger uncertainty in the result for AlSb is due to the poor surfaces of this material.

We also include in Table IV all of the previous measurements of  $\chi_{14}$ . Within the large experimental uncertainties there is agreement for crystals studied by more than one group.

TABLE IV  
MEASURED INTENSITIES AND CALCULATED SUSCEPTIBILITIES

	InP	GaAs	AlSb	GeP
$^+W_{2\omega}$	2.2 ± .4 volts	22 ± 2 volts	1.1 ± 0.7 volts	3.8 ± 1 volts
$^+W_{2\omega}^{KDP}$	22 ± 4 "	22 ± 4 "	21 ± 3 "	20 ± 2 "
$^-I_{\omega}$	12 ± 1 mv	23 ± 3 mv	12 ± 6 mv	9 ± 2 mv
$^+I_{\omega}^{KDP}$	40 ± 4 "	40 ± 4 "	28 ± 6 "	36 ± 2 "
$\chi_{14}$	$1.06 \times 10^{-6}$ esu (± 30%)	$1.21 \times 10^{-6}$ esu (± 30%)	$0.31 \times 10^{-6}$ esu (+ 75%)	$0.26 \times 10^{-6}$ esu (+ 35%)
$\chi_{14}^C$	0.76 "	1.07 "	0.25 "	0.18 "
$^* \chi_{14}^B$	—	1.20 " (+ 50%)	—	—
$^{**} \chi_{14}^G$	—	0.87 "	—	—
$^{***} \chi_{14}^S$	—	1.53 " (+ 50%)	—	0.25 " (+ 50%)

+ Peak intensities as measured on oscilloscope with 10 kΩ load.

\* Ref. N. Bloembergen, R. K. Chang, J. Ducuing, P. Lallemand (presented at Semiconductor Physics Confer., Paris, 1964).

\*\* Ref. M. Garfinkel, W. E. Engeler, *App. Phys. Lett.*, **3**, 178 (1963)  
(Note: Authors erroneously give value of  $2.6 \times 10^{-6}$  esu; using their data and formula, we obtained  $0.87 \times 10^{-6}$  esu).

\*\*\* Ref. R. A. Soref, H. W. Moos, *J. App. Phys.*, **35**, 2152 (1964).

## E. DISCUSSION

Second harmonic generation in four members of the III-V family of semiconductors (InP, GaAs, AlSb, and GeP) was observed for excitation by a Q-switched Nd<sup>3+</sup> glass laser. We have observed this radiation for the first time in AlSb and InP. Since these substances are opaque at the harmonic frequency, the emission was generated in the surface layer of ~ 1000-Å thickness at the exit faces of these crystals.

From the measured intensities we have calculated the nonlinear susceptibility coefficient of these compounds. For GaAs and GeP, which have been studied before, our values are within experimental error of those reported previously. The large discrepancies between the theoretical

curves for the orientational dependence of the harmonics and the experimental points is probably due to irregularities and inhomogeneities in the surface structure which would cause deviations from the bulk crystal symmetry in the very thin radiating layer. The bulk symmetry is still remarkably preserved within a thickness of  $\sim 1000 \text{ \AA}$  of the surface. The fluctuations in the harmonic intensities from successive laser pulses is probably due in a large measure to the corresponding variations in the coherence properties of the complex multimodal laser emission. Consequently, it appears that the method which should be employed to obtain the most accurate value of the nonlinear susceptibility would utilize a focussed continuous gas laser for the excitation source. Since gas lasers can be operated in relatively simple modes this would eliminate coherence fluctuations. For a 0.1-watt laser focussed to an area of  $10^{-6} \text{ cm}^2$ , the power density would be equivalent to that used in our experiment. The use of a narrow-band lock-in amplifier arrangement would increase signal to noise by almost a factor of 1000 over our values. The only difficulty would be the greater complexity of the analysis of the propagation of a highly convergent beam in a nonlinear medium.

Our results can be analyzed in terms of the quantum mechanical treatments for second harmonic generation in insulators and semiconductors developed by Butcher and McLean<sup>20</sup> and Kelley,<sup>21</sup> among others. Soref<sup>13</sup> and Soref and Moos<sup>12</sup> have derived from the above treatments relationships between band structure and the nonlinear susceptibility coefficients. For a simplified model consisting of spherical conduction and valence bands having equal effective masses, assuming vertical electric dipole transitions at  $k = 0$ , the above-mentioned investigators found that the nonlinear susceptibility depends strongly on the parameter  $(E_g - 2\hbar\omega)/\hbar\omega$ . They found very good experimental agreement with this dependence for the alloy system CdSe-CdS-ZnS which has band gaps varying from 1.71 eV to 3.56 eV, and for which this parameter varies between -0.59 and 1.04 for the Nd<sup>3+</sup> laser. The most interesting feature of both the calculated and measured susceptibilities is that as  $(E_g - 2\hbar\omega)/\hbar\omega$  decreases from 1 to 0,  $\chi$  increases slowly. However, when  $E_g = 2\hbar\omega$  the increase of  $\chi$  with a decrease in this parameter becomes much greater and continues to rise steeply for the smallest band gap material that Soref and Moos studied. Our value of  $\chi_{14}$  for GaAs, AlSb, and GaP can also be fitted by the curve derived by Soref and Moos. In fact, to do so, we must assign to AlSb a direct band gap of  $2.3 \pm 0.3 \text{ eV}$ , a parameter which has as yet not been measured directly. Hence, for these materials, the simple band structure model is adequate for explaining our results. However, our value for  $\chi_{14}$  for InP, as well as those obtained by Bloembergen et al.<sup>11</sup> for GaSb, InAs and InSb are much smaller than predicted by the dependence of  $\chi_{14}$  on  $(E_g - 2\hbar\omega)/\hbar\omega$ . In fact, the nonlinear susceptibility appears to oscillate about an approximate value of  $1 \times 10^{-6} \text{ esu}$  for values of the above parameter smaller than -0.9. To explain this behavior as well as the dispersion in  $\chi_{14}$  measured by Bloembergen et al. will require a more complicated band structure model than has been used so far.

### III. FREQUENCY MIXING IN SEMICONDUCTORS

#### A. INTRODUCTION

Magneto- and electro-optic effects have usually been studied where the E- and H-fields are statically applied and an incident radiation field merely causes electronic transitions between levels. In semiconductors and insulators, the intrinsic absorption edges are displaced by the application of static E-fields of approximately  $10^5$  cm. When an external H-field of approximately  $10^4$  gauss is applied to semiconductors, the valence and conduction bands split into Landau levels and oscillatory-absorption structure is observed. The electronic nature of these effects would indicate that if high optical E- and H-fields are incident upon a semiconductor, the radiation field could cause a mixing of levels as well as electronic transitions between levels with the consequence that the real and imaginary parts of the absorption could respond to the difference frequency due to the presence of two optical frequencies incident in the neighborhood of the absorption edge of the semiconductor. The possibility of observing such nonlinearities was discussed in a previous publication.<sup>1</sup>

While instrumentation was being assembled to study this type of nonlinear interaction, observations of optical frequency-mixing in bulk CdSe<sup>2,3</sup> were reported. In these experiments, the axial modes of a ruby laser were mixed to obtain microwave power in the 1 to 5 Gc/sec region. The microwave power was found to be proportional to the square of the applied bias and the incident intensity. This was also indicated in our work. The frequency-mixing could possibly be interpreted as a manifestation of the previously proposed nonlinear interband field effect. However, since the axial modes overlapped the bandgap, the resultant carrier generation rate could be modulated at the difference frequency and the application of a constant electric field to the sample could cause microwave power to be radiated; consequently, the observed effect could be interpreted in terms of a photoconductive mechanism rather than in terms of a nonlinear interband effect.

It can be shown that in the case of mixing produced by shifting of the band edge by a high-frequency E-field (the shift of the band edge is independent of the direction of the E-field), it would be necessary to apply an external bias field to observe the difference frequency. The expected power at the difference frequency would be proportional to the square of the bias field and the incident intensity, thus, both photomixing and the interband mixing would have this common feature. The power produced by photoconductive interactions would, however, also be sensitive to the mobilities and lifetimes of the generated carriers while the nonlinear interband effect would be insensitive to these parameters. In addition, the latter interaction is expected to be relatively independent of the frequency difference between the two incident monochromatic beams, while the photomixing process would be markedly frequency-dependent.

To understand the mechanism responsible for the frequency-mixing in CdSe these observations were repeated and extended to Ge, GaAs, and Si using a ruby and Nd laser with each of these substances. Since these different laser sources overlapped appreciably different regions of the band edge, a nonlinear interband effect would yield differences in microwave output for each source while for a photoconductive mechanism little difference would be anticipated.

The results obtained from these experiments substantiate the interpretation that the observed effects were due to photoconductive mixing and not to any nonlinear effects associated with a shift in the absorption edges in these substances. This conclusion is also substantiated by other work.<sup>22-25</sup>

Concomitant with this phase of the work a study was made of the frequency-tuning of GaAs lasers by uniaxial stress. The initial results of this study were published,<sup>26</sup> a reprint of which is included in Appendix II. It was demonstrated that the frequency of a GaAs injection laser would be readily tuned through 1% of its frequency. The use of uniaxial stress was also shown to be a useful parameter for studying the nature of electronic transitions involved in the emission processes from semiconductors. The work on frequency-mixing in semiconductors and stress-tuning of injection lasers indicates the possibility of producing tuneable power at high microwave frequencies. This could be realized by mixing the frequencies of two different lasers, one derived from a stress-tuned diode the other from an unstressed source on an appropriate semiconductor. This work is discussed in the final part of this report.

## B. EXPERIMENTAL ARRANGEMENT

The difference frequencies produced by the mixing of the axial modes of a ruby or  $\text{Nd}^{3+}:\text{CaWO}_4$  laser in CdSe, Si, GaAs, and Ge were coupled to a coaxial transmission line and detected by conventional rf techniques. The optical lasers employed were of the non-Q switched variety; peak powers in the neighborhood of 30 to 100 watts were incident upon the materials. The sample dimensions were  $2 \times 2 \times 0.2$  mm with the surfaces facing the incident laser beam etched with appropriate low surface recombination etches. The semiconductors were connected between the central and outer conductors of the coaxial transmission line by means of nickel tabs which were resistance-soldered to the semiconductors. A biasing field was applied across the 2-mm length of sample by means of dc-blocking capacitor. A high-pass rf filter was placed between the coaxial line and the rf-detecting system to block the low-frequency photoconductive signal conductors and to pass the microwave signal initiated by the laser pulses. The microwave power was detected by a crystal detector or spectrum analyzer depending upon the appropriate levels of microwave power. The power was determined by the use of calibrated attenuators. The ruby laser crystal was 7.8 cm long; if one takes the index of refraction ( $n = 1.76$ ) for ruby, the predicted axial mode separation  $\Delta\lambda = c/2nL = 1.092 \times 10^9$  cps, which compares with the lowest detected beat frequency of  $1.064 \times 10^9$  cps. The  $\text{Nd}^{3+}$  laser was a  $\text{CaWO}_4$  crystal containing 1% Nd and was

5.06 cm long. The predicted axial mode separation was  $1.54 \cdot 10^9$  cps while the observed axial mode separation was  $1.537 \cdot 10^9$  cps. The observed and predicted mode separations are in reasonable agreement considering the errors in  $n$  and  $L$ . The  $\text{Nd}^{3+}$  laser had a sufficiently low threshold so that it was possible to operate it at a repetition rate of 1 per 3 sec as compared to 1 per 20 sec for the ruby laser.

Figure 9 shows the block diagram of the experimental arrangement. So as not to heat the sample at high bias fields or when using low-resistivity samples, the bias fields were applied in square pulses only during the time when the laser signal was on. The laser flashlamp and relay for the bias were triggered from a common source with a variable delay amplifier in the bias channel so as to enable the field to be applied in approximate coincidence with the laser signal. When measurements as a function of laser intensity were performed, the flashlamp voltage was kept fixed and the light incident upon the samples was attenuated by calibrated wire mesh and neutral density filters. The laser output was monitored by reflecting a portion of the beam into an RCA-7102 photomultiplier. The monitored laser signal and generated microwave signal were each displayed on the channels of a dual-beam oscilloscope.

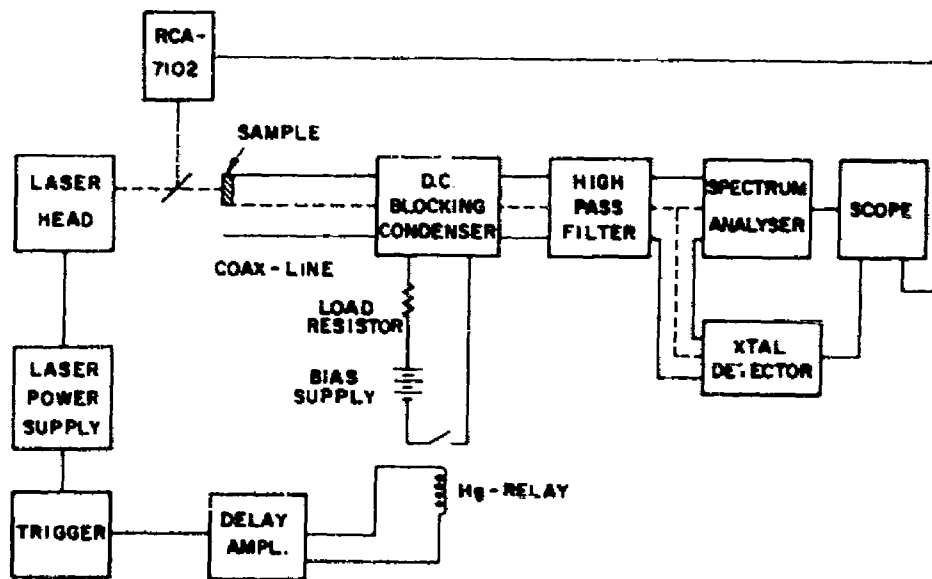


Fig. 9. Schematic diagram for detecting microwave beat frequencies.

The schematic diagram of the pulse amplifier, time delay amplifier, and relay circuit for trigger the laser flash lamp and bias circuit is shown in Fig. 10. The reed of the Hg relay had a delay of  $\sim 10^{-3}$  seconds but with less than a microsecond of time-gitter. The pulse delay circuit was made up of three identical channels, each with a variable delay time from 20-300  $\mu$  seconds which could be used in series. This delay time together with the delay between the exciting of the flashlamp and the initiation of the laser spikes were sufficient to enable time coincidence to be

obtained between the bias pulse and laser signal. The pulse amplifier and pulse time delay circuit excluding the relay circuit were also successfully used to trigger two independent lasers and obtain time overlap of the laser signals.

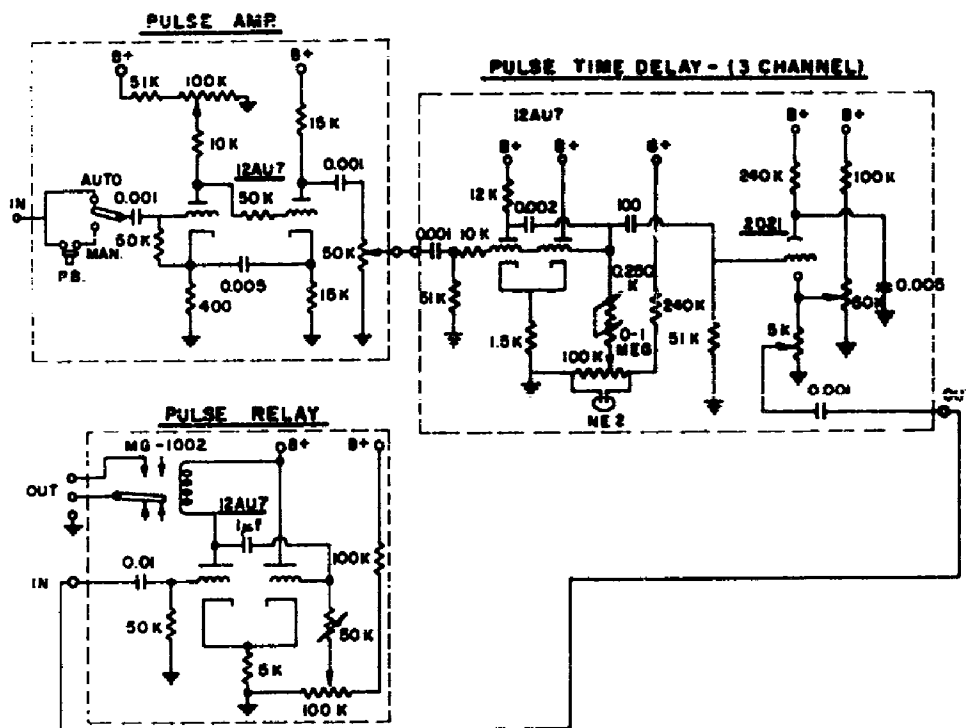
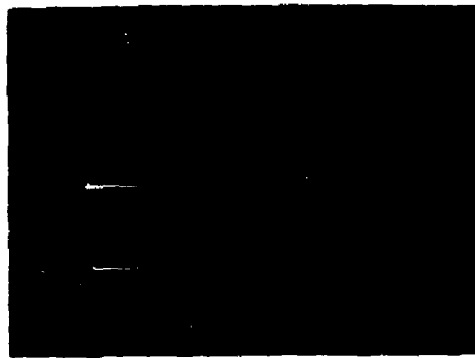


Fig. 10. Circuit diagram of pulse amplifier, time delay amplifier and relay for triggering laser and bias.

### C. EXPERIMENTAL RESULTS

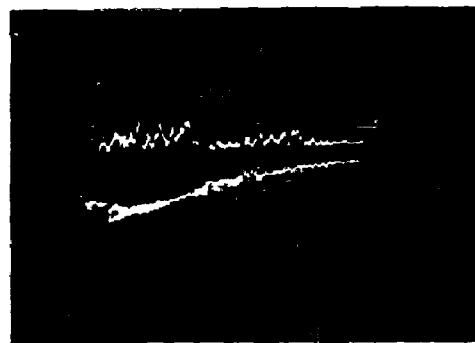
Typical experimental results for GaAs with a ruby laser are shown in Fig. 11a. The upper trace shows the laser output as monitored by the photomultiplier and the lower trace shows the rectified microwave signal. The duration of the microwave spikes were of the order of  $10^{-6}$  seconds. The frequency width of the microwave signal was of the order of 1 Mc/sec as measured with the spectrum analyzer, indicating that the width was determined by the Fourier components of the laser spike modulation. It should be noted that there are very few microwave spikes compared to laser spikes without direct correlation of the intensities of the respective signals. The fact that mixing does not occur for each coherent burst of the optical signal indicates the likelihood that spatial and temporal coincidence is not realized for each of the axial modes. Due to the random nature of the ruby and microwave signals, a great number of points were taken for a given experimental condition to obtain an average signal.



(a)



(b)



(c)

**Fig. 11. Correlation between microwave and exciting laser signal.**

- a. The upper trace is the ruby laser and the lower trace is the 1.064-Gc signal from GaAs with sweep speed of  $100 \mu \text{ sec/cm}$ .
- b. The 1.537-Gc signal from Ge excited by a Nd laser; the upper trace shows the microwave signal while the lower trace displays the laser signal with sweep of  $100 \mu \text{ sec/cm}$ .
- c. Same experimental conditions as (b) but with sweep of  $50 \mu \text{ sec/cm}$ .

The rf signals were found to depend upon the impedance mismatch between the samples and the transmission line. The dc resistance of the GaAs samples was  $\sim 10$  megohms. At high light levels where the photoconductivity was large compared to the sample dark conductivity, the amount of mismatch depended upon the light levels. The microwave signal was optimized by use of a double-stub tuner in such cases.

The microwave output power for GaAs with the ruby laser as a function of light intensity and bias are shown in Fig. 12. It is seen that within experimental error, the signal varies as the square of both the bias field and the intensity. The absolute value of the signal was found to be sensitive to surface treatment. Marked increases in signals were obtained when the surfaces facing the incident laser beam were etched with an appropriate low surface recombination etch. All the surfaces of Ge, Si, and GaAs used in these experiments were so etched.

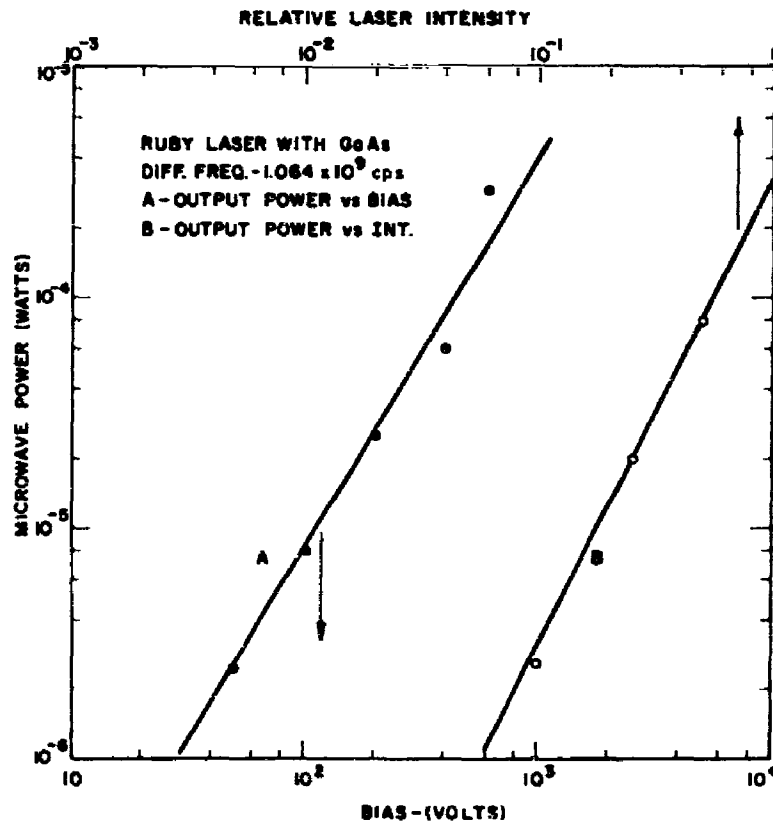


Fig. 12. Microwave power output vs. bias and laser intensity for GaAs with ruby laser.

The  $1.0 \times 10^9$  /sec signals from Ge using the  $\text{Nd:CaWO}_4$  laser are shown in Fig. 11b; the upper trace shows the microwave signal while the lower trace shows the laser signal. A time-expanded scale under the same experimental conditions is displayed in Fig. 11c, where again it is seen that there is no direct correlation between the intensity of the microwave and laser signals.

The peak microwave power for Ge with the  $\text{Nd}^{3+}$  laser as a function of bias is shown in Fig. 13. The signal varied as the square of the bias voltage up to approximately 200 volts beyond which value it breaks into a sublinear dependency and approaches a saturation value; the bias was applied across 2 mm of the sample, i.e., the field at which the break occurred was 1000 V/cm. Although the sample resistance was 500 ohms, the bias was applied for a time duration  $\sim 10^{-3}$  seconds to obviate excessive joule heating of the sample. Since the  $\text{Nd}^{3+}:\text{CaWO}_4$  laser could be operated at a repetition rate of 1/3 sec, the taking of a sufficient number of data points to delineate the shape of this curve was greatly facilitated.

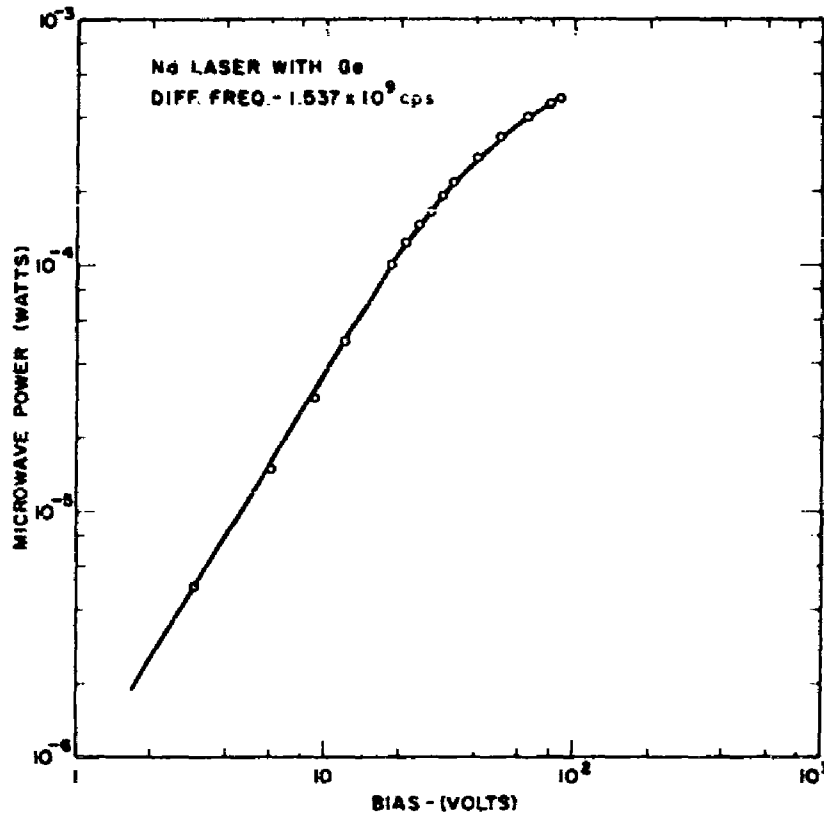


Fig. 13. Microwave power from Ge with  $\text{Nd}^{3+}$  laser as a function of bias.

To further explore this saturation effect observed in Ge, measurements were made on the mixing in Si with a ruby laser. The Si samples were compensated and had a room temperature resistance of approximately 10,000 ohms. The output signal versus bias curves at 300 K and 78°K are shown in Fig. 14. These results show a quadratic dependency of the signal on bias for fields up to 1000 V/cm after which they again tend to saturate as with Ge. The increase in output power by a factor of  $\sim 400$  for the sample temperature of 78°K relative to that at 300°K should be noted. The sample resistance was  $\sim 10,000$  ohms at 300°K and increased to more than 100 megohms at 78°K. It is unlikely that the saturation of the signal at the high fields is caused by an increase in temperature of the Si samples due to joule heating as was the possibility with the low-resistance Ge samples.

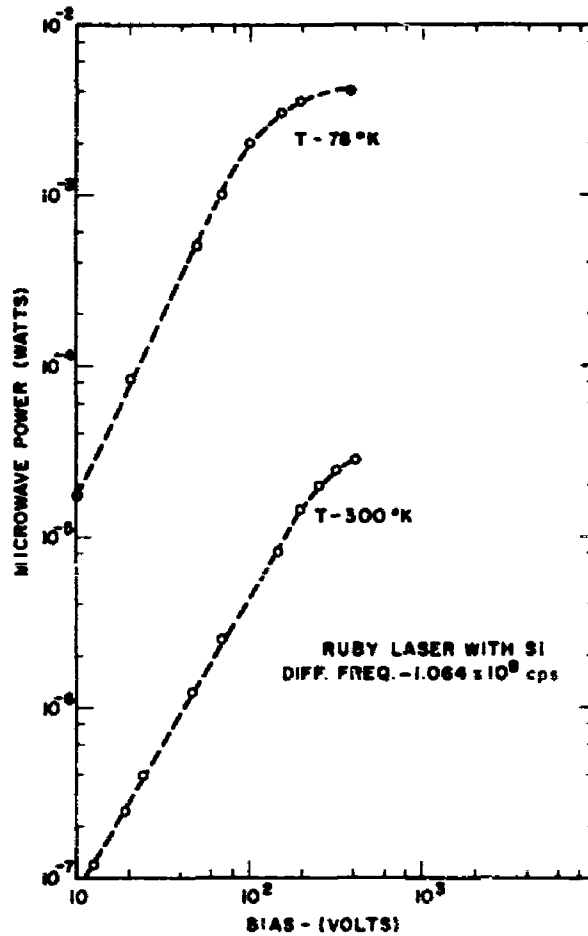


Fig. 14. Microwave power from Si with ruby laser vs. bias at 300°K and 78°K.

Equivalent data on the bias and intensity dependence of the signal using both the ruby laser as well as the Nd laser on Ge were obtained; the output power was approximately the same in both cases. Since each of these frequencies lie at appreciably different points of the Ge absorption edge, it seems likely that the frequency-mixing is due to a photoconductive process and is not engendered by nonlinear effects due to the shift of the band edge. A comparison was also made of the relative power outputs at the first, second, and third difference frequencies of the Nd modes on Ge with the result that the output signal was found to be proportional to the inverse square of the difference frequency. These results further indicate that the frequency mixing is due to photomixing effects.

#### D. THEORY OF PHOTOCONDUCTIVE FREQUENCY MIXING

The qualitative features of the experimental results reported in the previous section seem to indicate that the frequency-mixing in these semiconductors can be interpreted in terms of a mechanism involving pair creation by the axial modes of a laser. In this section, we shall develop the theory for a photoconductive frequency-mixing process and shall then compare the theory with the observed results. This problem has also been treated by a number of authors.<sup>23,25</sup>

When two monochromatic beams of slightly different frequencies are incident upon a semiconductor where electron-hole pairs can be photoexcited, the generation rate of free carriers will contain frequency components made up of the sum, difference, harmonics, and dc components of the incident frequencies. The mixed frequencies result from the fact that incident light intensity will be proportional to the square of the sum of the incident fields. In the case of optical frequencies, one can neglect the contributions of the harmonic and sum frequencies since the generated minority carriers cannot respond to these frequencies. Consider two similarly polarized monochromatic optical beams of photon energies  $\hbar\omega_1$ , and  $\hbar\omega_2$ , spatially and temporarily coincident upon a semiconductor surface of area  $xy$  and absorption coefficient  $K$ . The rate of generation of electron-hole pairs at depth  $z$  can be calculated from the continuity equation:

$$\frac{dN(z,t)}{dt} = K \left[ F_1 + F_2 + 2 \sqrt{F_1 F_2} e^{i\omega_3 t} \right] e^{-kz} - \frac{\eta}{\tau} \quad (23)$$

where  $\tau$  is the minority carrier lifetime,  $\omega_3 = \omega_1 + \omega_2$ , and  $F_1$  and  $F_2$  are the corresponding fluxes in photon/sec/cm<sup>2</sup> of the respective beams. Performing the integration with respect to  $t$  we obtain:

$$N(z,t) = \frac{K \tau e^{-kz} (F_1 + F_2)}{xy} + \frac{2 K \tau \sqrt{F_1 F_2} e^{-kz} e^{-i\omega_3 t}}{xy [1 + i\omega_3 \tau]} \quad (24)$$

If we allow  $\eta$  to represent the fraction of incident photons effective in creating electron-hole pairs within the bulk of the semiconductor, the integration over  $z$  can be performed by replacing the terms  $K e^{-kz}$  by  $\eta$ . If we take the real part of Eq. (24), we obtain

$$N(t) = \frac{\tau \eta (F_1 + F_2)}{xy} + \frac{2 \tau \eta \sqrt{F_1 F_2} \cos(\omega_3 t + \phi)}{xy [1 + (\omega_3 \tau)^2]^{1/2}} \quad (25)$$

where  $\phi = \tan^{-1} \frac{1}{\omega \tau}$

When a dc bias field  $E_B = v/x$  is applied to the sample a current  $I = N \mu E_B y z$  will flow which is given by

$$I = \frac{r \mu e \eta [F_1 + F_2] E_B}{x} + \frac{2 r \mu e \eta \cos(\omega_3 \tau + \phi)}{x [1 + (\omega_3 \tau)^2]^{1/2}} \quad (26)$$

The first term is the dc photocurrent while the second term is the microwave current. If the sample output is terminated in a matched load  $R_L$ , the microwave power at the difference frequency  $\omega_3$  that can be radiated is given by

$$P_{\omega_3} = \frac{1}{2} R_L \left[ \frac{r \mu e \eta P_i E_B}{x \langle \hbar \omega \rangle [1 + (\omega_3 \tau)^2]^{1/2}} \right]^2 \quad (27)$$

where we have expressed the flux in terms of the total incident optical power of both beams and  $\langle \hbar \omega \rangle$  represents the mean photon energy of the optical beam. The radiated power is seen to be proportional to the square of the product of the incident power, bias field, and the mobility. If  $\omega_3 \tau \gg 1$ , the output power will be independent of the minority carrier lifetime and will vary inversely as the square of the difference frequency; while if  $\omega_3 \tau \ll 1$  the radiation will be independent of  $\omega_3$  but will in addition be dependent upon  $\tau^2$ . For high frequencies where  $\omega_3$  becomes comparable to the lifetime broadening of the initially excited carriers by electron-electron and electron-phonon interactions, the output power given by Eq. (27) will be further reduced.<sup>27</sup>

## E. DISCUSSION

The experimental results of the mixing of the axial modes of a ruby or a  $Nd^{3+}$  laser in CdS, Si, Ge, and GaAs have the common feature that the microwave output power is proportional to the square of the incident optical intensity and bias field and is inversely proportional to the square of the difference frequency. However, the absolute yields of the microwave power for a given optical power, bias, and frequency vary from substance to substance. These observations are in qualitative agreement with the theory for photomixing.

The quantitative experimental results shall now be compared with theory as given by Eq. (27). We shall assume that  $\omega_3 \tau \gg 1$  in Ge, Si, and GaAs which seems reasonable for the reported minority carrier lifetimes at these substances;  $\eta$  will be taken as 0.5 for all three semiconductors, which is equivalent to the assumption that the intrinsic quantum efficiency for pair creation is unity and that no surface recombination of the generated carriers occurs, and  $\eta$  is therefore determined by the reflection losses which are approximately 50% for these semiconductors. It will furthermore be assumed that 10 axial modes of equal intensity contribute to the optical power in both the ruby and  $Nd^{3+}$  laser.

For Ge with Nd, taking  $\mu = 3600 \text{ cm}^2/\text{V-sec}$  and a bias field of  $10^2 \text{ V/cm}$ , Eq. (27) predicts a power output of  $\sim 2 \times 10^{-4}$  watts as compared with the observed value of  $\sim 10^{-4}$  watts shown in Fig. 13. The predicted signal for Si with ruby using  $\mu = 1000 \text{ cm}^2/\text{V-sec}$  and  $E_B = 10^2 \text{ V/cm}$  is  $10^{-4}$  watts at  $300^\circ\text{K}$ , as compared with the  $2 \times 10^{-5}$  watts given in Fig. 13. The increase in signal by a factor of 400 for Si in going from  $300^\circ\text{K}$  to  $78^\circ\text{K}$  can be understood on the basis that the mobility increases by a factor of 10 for this temperature difference.<sup>28</sup> The observed signal from GaAs with ruby in Fig. 12 is  $8 \times 10^{-4}$  watts as compared with the predicted value of  $3 \times 10^{-5}$  watts for  $\mu = 3000 \text{ cm}^2/\text{V-sec}$  and  $E_B = 10^3 \text{ V/cm}$ . Thus we see that there is reasonable agreement between the observed and predicted microwave power. Since the reasonable assumption was made that  $\omega_3 \tau \gg 1$  in all these materials, the major difference in signal seems to be accounted for by the different mobilities. The influence of minority carrier mobility in determining the absolute values of the signal seems further substantiated by the saturation effects observed in Ge and Si at high bias fields which occur at  $\sim 1000 \text{ V/cm}$  where the drift velocities tend to saturate.<sup>29</sup>

The results of the optical frequency-mixing for the conditions of these experiments are in substantial agreement with the results expected for a photomixing mechanism. The possibility of observing optical frequency-mixing via nonlinear interband effects in semiconductors still remain to be investigated. However, the relatively high yields observed in the present work indicate the feasibility of extending these measurements to high frequencies. Work toward this end using injection lasers is discussed in the final part of this report.

## IV. FREQUENCY TUNING AND MIXING USING INJECTION LASERS

This work was partially supported by the contract funds as well as by RCA Laboratories' funds and was pursued in collaboration with D. Meyerhofer of this Laboratory.

### A. INTRODUCTION

Although presently available injection lasers have output powers of the order of watts, the power density in the neighborhood of the emitting junction is relatively high, thus warranting a consideration of the nonlinear processes that can take place in these materials. In the section on double-photon absorption (Section I-C), we have shown that this process can set an intrinsic upper limit to the output power obtainable from such devices. In addition, it is possible to observe internal second-harmonic generation in GaAs as a consequence of the high internal power densities.<sup>10</sup> Despite the relatively low total output power from such lasers, the fact that such sources can be used at relatively high repetition rates or in a cw fashion can be an appreciable advantage in narrow-banding the measurements for improved signal-to-noise in these studies.

In this phase of the program, a study was made of some of the characteristics of GaAs injection lasers that are pertinent to frequency-mixing operations. The modal structure of the laser frequencies and the output power from diodes fabricated by various techniques were examined. It was demonstrated that the frequency of GaAs injection lasers can be readily tuned through 0.5% of its frequency by the application of uniaxial stress. The use of uniaxial stress was also shown to be a useful parameter for studying the nature of the electronic transitions involved in the emission process.

The study of the photoconductive mixing in semiconductors at 1 Gc/sec (Section III) has indicated the feasibility of producing tuneable power at much higher frequencies. This could possibly be realized by mixing the frequencies of two different injection lasers, one frequency derived from a stress-tuned diode, the other from an unstressed diode in an appropriate semiconductor. Progress toward this end will be discussed in this part of the report.

### B. FREQUENCY-TUNING BY UNIAXIAL STRESS

The energy levels and, consequently, the frequency of the light emitted by a solid can be changed by stress. Use of uniaxial stress for changing the laser frequency has the advantage over other methods (hydrostatic pressure,<sup>30</sup> magnetic field<sup>31</sup>), in that the auxiliary equipment can be made simpler and smaller. In addition, the application of uniaxial stress to semiconductors generally splits energy levels which are degenerate in the absence of stress and so can be used as a means of identifying recombination processes. We have studied the effect of uniaxial stress on the frequency spectrum of spontaneous and stimulated light emitted from GaAs

laser diodes, and have obtained preliminary information about the nature of the electronic transitions responsible for the emission in such diodes. In particular, different emission processes seem to be taking place in diodes made from different materials.

The experimental arrangement is shown in Fig. 15 as is the crystallographic orientation of the diodes used. The compression is applied perpendicular to the plane of the junction which is a (100) plane. Other orientations would give additional information, but suitable diodes were not available. The diodes were in the shape of parallelepipeds, with typical dimensions of  $0.6 \times 0.16 \times 0.10$  mm, and had cleaved sides.

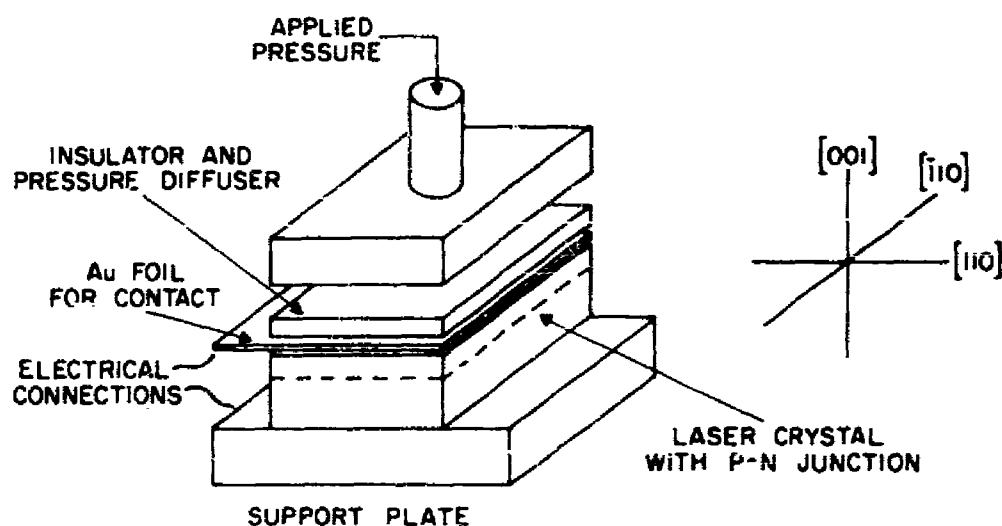


Fig. 15. Experimental arrangement for the compression measurements; the crystallographic orientation of the GaAs diodes used is indicated at the right.

The effect of uniaxial compression on the coherent emission of a typical laser diode is shown in Fig. 16. The emission lines are not single resonant modes of the diode, but rather envelopes of a number of such modes. Unfortunately, samples small enough, so that individual modes could be resolved (separation of  $2 \text{ \AA}$  for the longitudinal modes), were too fragile for stress measurements. Both shifts of the location of the envelopes with uniaxial stress as well as "moding" from one set of envelopes to another have been observed. These frequency changes are not necessarily linear with stress, as can be seen in Fig. 16, where the curve at the highest stress lies between the other two. The maximum shift of the laser line in this diode was  $20 \text{ \AA}$  or 0.25% in frequency. In some diodes it was found that the envelope curves narrowed with increasing stress, suggesting that fewer modes "lased" under this condition.

The results for coherent emission varied from diode to diode since they depend on both changes in the emitting transitions, as well as on changes of the resonant cavity. The interpretation of the data is therefore more complicated since it requires the knowledge of the individual cavity modes. We therefore also studied the incoherent light emission which should only depend on the electronic transition.

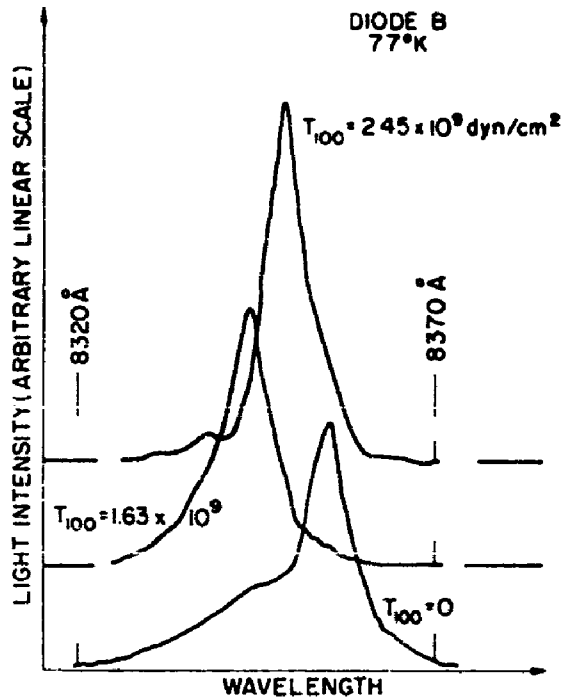


Fig. 16. Reconder trace of the coherent emission line from a GaAs diode at three different stresses. The curves are displaced vertically for clarity. The linewidths are due to the unresolved modes. (Instrumental resolution  $\sim 1 \text{ \AA}$ .)

The shape of the incoherent emission line was found to be independent of the applied stress, and the only variable is the frequency of the light. This change of energy is plotted in Fig. 17 as function of the uniaxial compressive stress for three different diodes. It is clear that the three diodes, which were made in different ways, show very different behavior: the frequency of A increases linearly with stress, while B and C show saturation and even negative changes. Other diodes, made in the same way as A, B, or C, do reproduce the respective curves. It should be noted that frequency shift of diode B is the same for coherent and incoherent emission.

Diode A was made by solution-growing an n-layer with a doping of  $\sim 1 \times 10^{18}/\text{cm}^3$  Sn atoms on a crystal with  $1 \times 10^{19}$  Zn atoms/ $\text{cm}^3$ , with subsequent diffusion to form a graded junction. This diode did not "lase." Diodes B and C were also made by solution growth and diffusion, but the grown region was doped with both Sn and Te to a total concentration of  $1 \times 10^{18}/\text{cm}^3$ . They were grown on two different crystals with approximately the same doping. All such diodes showed lasing behavior, with the lasing frequency at the peak of the incoherent emission. The peak of the emission of all three kinds of diodes was located at approximately the same energy (1.47 eV).

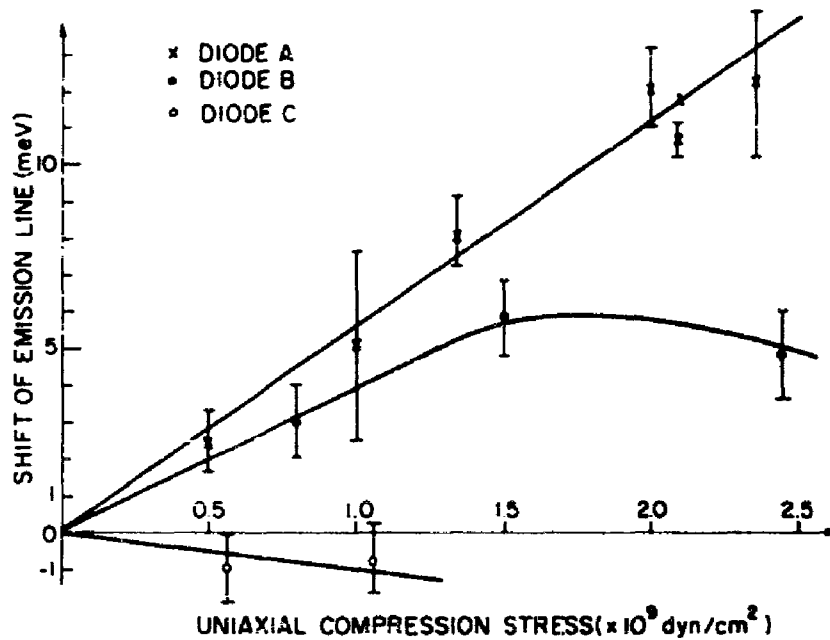


Fig. 17. Shift of the incoherent emission line from three typical GaAs diodes with uniaxial compression stress at 78°K. The indicated spread of the individual data points represents the variation of the results of all the measurements made at a given stress.

If the emission is due to band-to-band recombination or recombination via an exciton, then one can calculate that the emission line is both shifted in its average value and split due to strain.<sup>32</sup> For simplicity we shall assume that the band structure of GaAs at  $k = 0$  is similar for that of Ge and, consequently, shall employ the theory as was developed for Ge.<sup>33</sup> For the crystallographic orientation used in our experiments, the mean energy shift is

$$\bar{E} - E_0 = (D_d^c - D_d^v) \frac{T_{100}}{C_{11} + 2C_{12}} \quad (28)$$

and the splitting

$$2\Delta = 4/3 D_u \frac{T_{100}}{C_{11} - C_{12}} \quad (29)$$

in the notation of Kleiner and Roth.<sup>33</sup>  $T_{100}$  is the applied stress. The quantity  $(D_d^c - D_d^v)$  for GaAs can be determined from the effect of hydrostatic pressure on absorption measurements,<sup>34</sup> or from emission measurements<sup>30</sup> or from the effect of shear stress on the absorption.<sup>35</sup> The various values average out to  $9 \pm 2$  eV. The quantity  $D_u$  has not been measured in GaAs. Values for germanium are estimated at 0.3 eV,<sup>32,36</sup> and we expect similar values to apply for GaAs because of the similarity of the valence band structures of the two materials. In that case  $2\Delta$  becomes 1.5 meV for  $2.5 \times 10^9$  dyn/cm<sup>2</sup>, our largest stress.

Diode A (Fig. 17) does appear to follow the behavior predicted by Eqs. (28) and (29). The energy changes linearly with stress and no splitting is observed (1.5 meV would be too small to observe). We can calculate  $(D_0^c - D_0^v)$  from the slope of the straight line and the known elastic constants<sup>37</sup> and we obtain a value of  $12.5 \pm 2$  eV in agreement with the previous measurements. This suggests that the transition in diodes of the type A is either a band-to-band transition, or a transition to an impurity level which is tightly bound to one of the bands and does not split substantially under stress.

On the other hand, the behavior of type B and C diodes can certainly not be explained by the simple model. Rather, the emission appears to take place between energy levels that are more complicated. These may be shifting relative to the band edges or more complicated splittings may occur. A detailed interpretation of the nature of these centers will require further measurements on diodes with different dopings and stress orientations.

We have shown that uniaxial compression will shift the frequency of a GaAs laser by a substantial amount. We expect other injection lasers made from III-V compounds and alloys to show similar shifts, since the deformation potentials are expected to be of the same order of magnitude. Furthermore, uniaxial stress has been shown to be a very sensitive tool for studying the electronic transitions in light-emitting diodes.

The above measurements were made by employing a mechanical structure whereby a compressional force, through a rod and piston arrangement, was applied to the diodes which were immersed at the bottom of a liquid nitrogen dewar. Because of a certain amount of unavoidable friction between the piston and retaining cylinder, there is uncertainty of approximately 20% in the stress values, which led to scatter in the data and a consequent uncertainty in the frequency. In order to obtain more detailed measurements to elucidate the nature of the optical transitions as well as give finer frequency control, more refined stress equipment was designed and tested.

One structure comprised a piezo-electric crystal and laser diode clamped together, enabling the force to be applied by electrical means; this structure allowed a fine control of the frequency of the laser diodes by remote control. In order to measure the resultant stress, another piezo-electric element was included between the anvils containing the diode and stressing crystal. Although the above structure performed satisfactorily at low stress values, it could not be used at high stresses.

A structure employing He gas as the stress transfer medium was finally designed and tested which yielded satisfactory results. In this arrangement, shown in Fig. 18, the stress to the diode is applied by a piston-like arrangement which comprises a thin copper membrane under hydrostatic gas pressure. Extremely fine control of the stress is possible by control of the gas pressure from a tank external to the laser dewar.

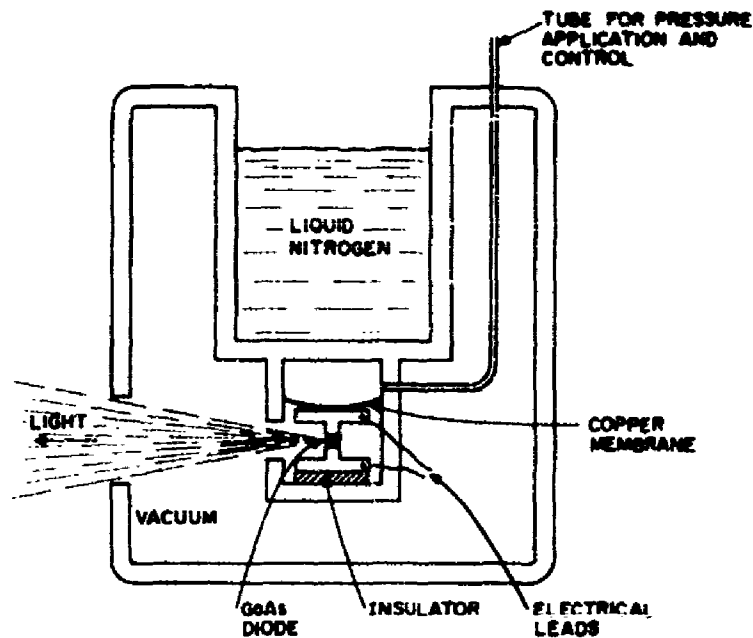


Fig. 18. Schematic diagram of uniaxial stress apparatus.

### C. PROPERTIES OF GaAs LASERS

Since little information was available regarding the modal structure, frequency stability, and power output for the diodes used in this work, some detailed studies of these characteristics were undertaken. The GaAs diodes were prepared by H. Nelson of these Laboratories either by diffusion or by solution-growth techniques; the more efficient diodes were grown by the latter technique. They were in the shape of rectangles, typically  $0.02 \times 0.05$  cm, with the shorter sides cleaned, the others sawed. The diodes were soldered onto copper or molybdenum holders which served as structural supports and a heat sink.

In frequency-mixing applications, it is necessary that the frequency of the emitted light, or the modes that are excited during lasing conditions remain constant with time. The driving pulse height was limited to a value which did not cause heating, so that the frequency distribution did not change during the pulse; this frequently has meant short pulses (less than 1- $\mu$ sec duration). The power output of many of these diodes were  $\sim 100$  mW with efficiency of  $\sim 1\%$ ; for these measurements a photomultiplier calibrated with a calorimeter was used. Improvements with respect to material and mounting procedures have enabled cw operation. In such cases, we have obtained freedom from frequency drift when the sample temperature reached a steady-state value.

The diodes varied considerably in their response, even for samples cut from the same wafer. Two of the quantities most easily measured were threshold current and efficiency of radiation at liquid nitrogen temperatures, and these quantities do not vary much among good diodes. When the light output as function of direction (far field pattern) was investigated, a

large amount of variation was observed. However, for diodes that had good resonant cavities an almost ideal pattern has been observed, which can be explained simply by diffraction effects of light emitted from a slab. The diffraction pattern is sketched in Fig. 19. The diode is represented

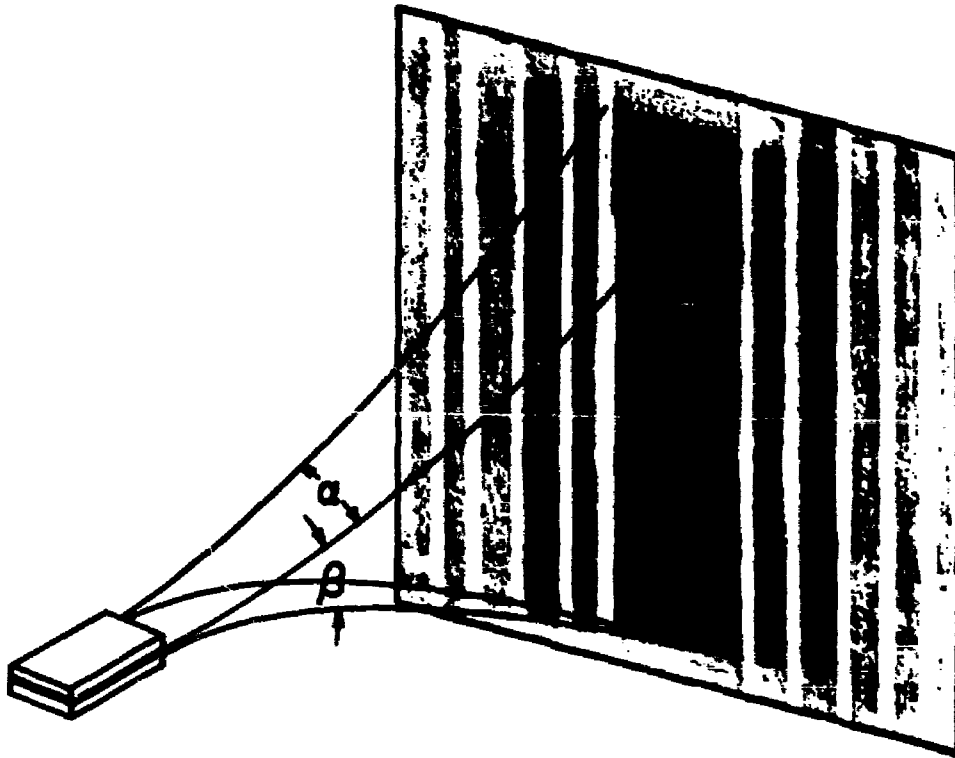


Fig. 19. Sketch of the far-field pattern of a GaAs diode with the simplest possible mode structure (diffraction effects).

by parallel light passing through a slot (the intersection of the active junction region with the crystal surface) of length  $a$  and width  $b$ . The length can be as long as the crystal face if the entire junction is oscillating in phase. The width will be related in a complicated way to the junction thickness.<sup>30</sup> The diffraction of the central maximum is given by

$$\sin \frac{\alpha}{2} = \frac{\lambda}{a}$$

$$\sin \frac{\beta}{2} = \frac{\lambda}{b} \tag{30}$$

A far-field picture of a GaAs diode is shown in Fig. 20. The central maximum is given approximately by  $\alpha = 2^\circ$ ,  $\beta = 90^\circ$ , so that  $a = 50\mu$ ,  $b = 1.2\mu$ . The length  $a$  is about one half of the actual width of the diode, so that the coherence region covers a large fraction of the junctions.

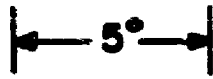
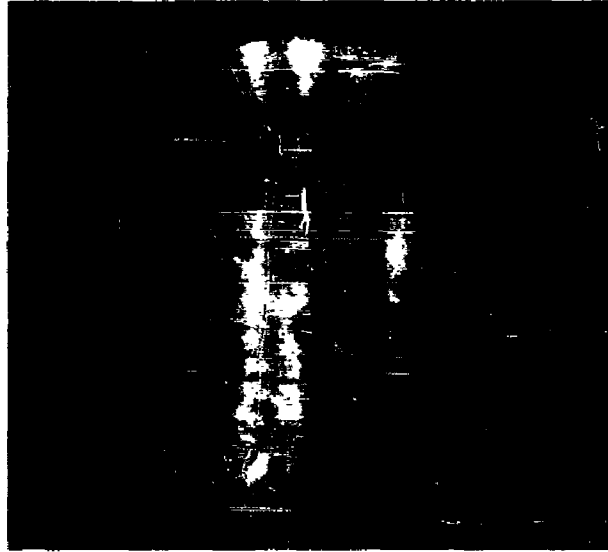


Fig. 20. Far-field pattern of GaAs laser diode.

#### D. MODAL STRUCTURE OF GaAs LASER EMISSION

The physical dimensions of a GaAs diode are very small compared with those of crystal or gas lasers with the consequence that the frequency separations are large in injection lasers. The distance between the reflecting mirrors is the length of the optical cavity  $l$ , and it primarily determines the mode structure of the laser. The frequency,  $\nu$ , of the possible modes is given by the relationship

$$\frac{\Delta\nu}{\nu} = \frac{1}{\nu} \frac{\partial\nu}{\partial m} = \frac{C}{\lambda} \frac{1}{2\left(n_r + \frac{\nu \partial n_r}{\partial \nu}\right)} \quad (31)$$

where  $m$  is an integer and  $n_r$  the index of refraction. The frequency difference between adjacent modes is then given by

$$\frac{\Delta\nu}{\nu} = \frac{1}{\nu} \frac{\partial\nu}{\partial m} = \frac{C}{\nu} \frac{1}{2\left(n_r + \frac{\nu \partial n_r}{\partial \nu}\right)} \quad (32)$$

or in terms of wave numbers

$$\frac{\Delta\nu}{C} = \frac{1}{2l\left(n_r + \frac{\partial n_r}{\partial \nu}\right)} \quad (33)$$

For GaAs at  $8400 \text{ \AA}$ ,  $n_r$  is 3.5 and  $\frac{\nu \partial n_r}{\partial \nu} \approx 1.5$ .<sup>39</sup> This shows that the wave number of the difference-frequency radiation produced by mixing of two adjacent modes is inversely proportional to the cavity length. For gas lasers  $\Delta/c$  is of the order of  $10^{12} \text{ cm}^{-1}$  or 300 Mc, for crystal lasers one order of magnitude higher, while typical injection lasers have the value  $\Delta/c = 3 \text{ cm}^{-1}$  or 100 Gc. This shows that mixing of modes of a single GaAs laser should produce radiation in the millimeter wave region.

To assess the mode structure, the intensity of the emitted light was measured as function of frequency; for most of the measurements a Perkin Elmer 112 grating spectrometer was employed; the resolution of the instrument was not sufficient to completely resolve the individual modes in most cases, and only a general indication of the number of oscillating modes can be obtained. Most of the available diodes have lasing modes distributed over  $\sim 10 \text{ \AA}$  (0.1% of the frequency) without any smooth distribution of intensity.

More detailed measurements on one diode have been taken with a Jarrel-Ash spectrometer of much higher resolution. The result of one run (at  $4.2^\circ\text{K}$ ) about 60% above threshold is shown in Fig. 21. At least 40 lines are observed. They fall into two groups of modes with equal spacing of  $1.3 \text{ \AA}$  between lines. The longitudinal mode spacing for this diode (0.56 mm wide) is calculated to be  $1.25 \text{ \AA}$ , which confirms the assignment of the lines. These same cavity modes are also observed below threshold in spontaneous emission. There the intensity distribution of lines is considerably smoother.

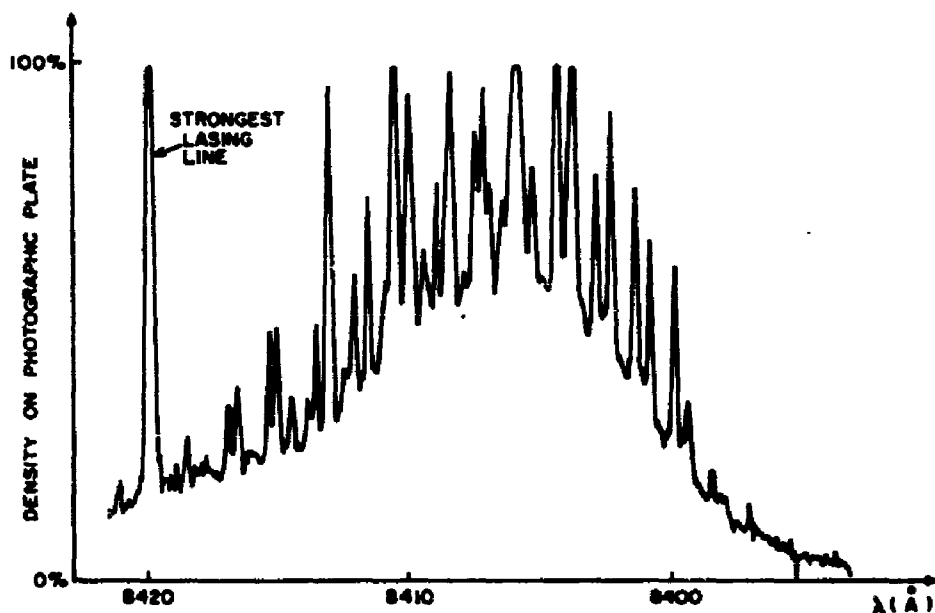


Fig. 21. High resolution spectrum of GaAs laser.

## E. MIXING EXPERIMENTS WITH LASER DIODES

The experimental arrangement for producing frequency-mixing in the microwave region employing laser diodes is shown in Fig. 22. The two laser diodes are each contained in separate dewars, the outputs of which are separately superimposed upon a semiconductor which is terminated in an appropriate waveguide. A single diode can be employed for the 1-3 mm region by mixing adjacent axial modes. When two separate diodes are employed it will be necessary to

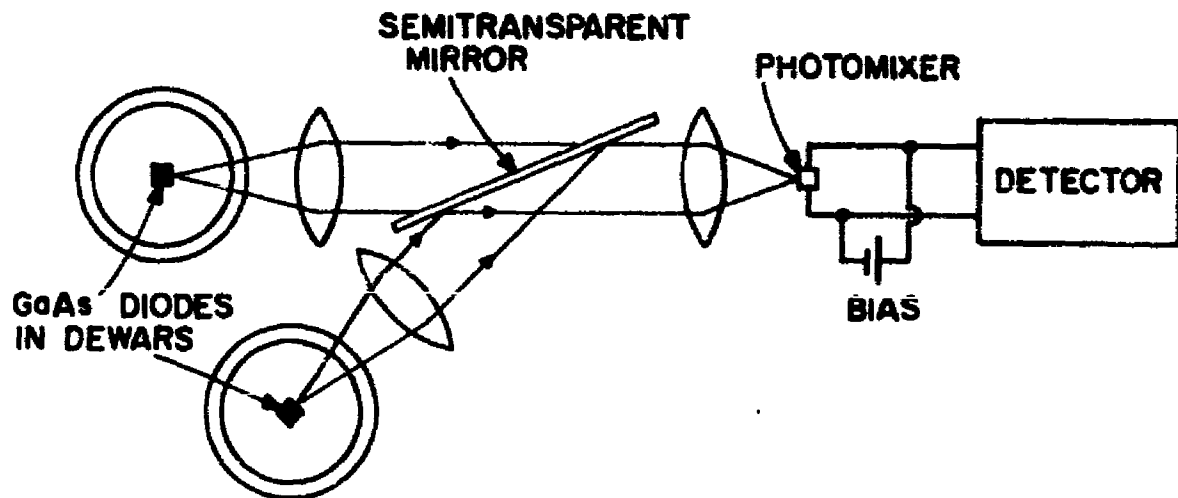


Fig. 22. Diagram of mixing experiment using two GaAs diodes.

stress-tune one of them to obtain appropriate difference frequencies in the 1-100-Gc region. If two arbitrary diodes are selected, it is found that the frequencies differ widely under unstressed conditions upon the doping level. The influence on doping on the emission was investigated, the results of which were published.<sup>40</sup> A reprint of this publication is included in Appendix III.

The essential instrumentation for these experiments has been completed and a search for radiation is to be initiated.

## REFERENCES

1. R. Braunstein, Phys. Rev. **125**, 475 (1962).
2. R. Braunstein and N. Ockman, Phys. Rev. **134**, A499 (1964).
3. W. Heitler, *The Quantum Theory of Radiation*, (Oxford University Press, second edition, 1954).
4. A. H. Wilson, *The Theory of Metals*, (Cambridge University Press, second edition, 1953).
5. E. O. Kane, J. Phys. Chem. Solids **1**, 245 (1957).
6. R. Braunstein and E. O. Kane, J. Phys. Chem. Solids **23**, 1423 (1962).
7. D. A. Kleinman, Phys. Rev. **125**, 87 (1962).
8. P. A. Franken, A. E. Hill, C. W. Peters and G. Weinreich, Phys. Rev. Letters **8**, 18 (1962).
9. J. Ducuing and N. Bloembergen, Phys. Rev. Letters **10**, 474 (1963).
10. M. Garfinkel and W. E. Engeler, Appl. Phys. Letters **3**, 178 (1963).
11. N. Bloembergen, R. K. Chang, J. Ducuing, and P. Lallemand, International Conference on the Physics of Semiconductors, Paris, July 1964.
12. R. A. Soref and H. W. Moos, J. Appl. Phys. **35**, 2152 (1964).
13. R. A. Soref, Tech. Report No. 0556-8, Electron Devices Laboratory, Stanford Electronic Laboratory, Dec. 1963.
14. N. Bloembergen and P. S. Pershan, Phys. Rev. **128**, 606 (1962).
15. D. A. Kleinman, Phys. Rev. **128**, 1761 (1962).
16. A. Ashkin, G. D. Boyd, and J. M. Dziedzic, Phys. Rev. Letters **11**, 14 (1963).
17. J. Dennis and H. Kingston, Appl. Optics **2**, 1334 (1963).
18. J. Ducuing and N. Bloembergen, Phys. Rev. **133**, A1493 (1964).
19. R. K. Chang, Harvard University (private communication).
20. P. N. Butcher and T. P. McLean, Proc. Phys. Soc., London **81**, 219 (1963).
21. P. L. Kelley, J. Phys. Chem. Solids **24**, 607 (1963).
22. R. H. Pantell, M. DiDomenico, Jr., O. Svelto, and J. H. Weaver, Proceedings of Third Intn'l. Conf. on Quantum Electronics, Paris, France, (1963).
23. G. J. Lasher and A. H. Nethercot, Jr., J. Appl. Phys. **34**, 2122 (1963).
24. G. Lucovsky, R. Schwarz, and R. Emmons, Proc. IEEE (correspondence) **51**, 613 (1963).
25. O. Svelto, P. D. Coleman, M. DiDomenico, Jr., and R. H. Pantell, Proceedings of Third Intn'l. Conf. on Quantum Electronics, Paris, France, (1963).
26. D. Meyerhofer and R. Braunstein, Appl. Phys. Letters **3**, 171 (1963).
27. P. S. Pershan and M. Bloembergen, Appl. Phys. Letters **2**, 117 (1963).
28. G. M. Ludwig and R. L. Watters, Phys. Rev. **101**, 1699 (1956).
29. E. Conwell, J. Phys. Chem. Solids **8**, 234 (1959).

## REFERENCES (Continued)

30. J. Feinleib, S. Groves, W. Paul, and R. Zallen, *Phys. Rev.* **131**, 2070 (1963).
31. F. L. Galeener, G. B. Wright, W. E. Krag, T. M. Quist, and H. J. Ziegler, *Phys. Rev. Letters* **10**, 476 (1963).
32. G. E. Pikus and G. L. Bir, *Phys. Letters* **6**, 103 (1961).
33. W. H. Kleiner and L. M. Roth, *Phys. Rev. Letters* **2**, 334 (1959).
34. W. Paul, *J. Appl. Phys.* **32**, 2082 (1961).
35. M. D. Sturge, *Phys. Rev.* **127**, 768 (1962).
36. S. H. Koenig and J. J. Hall, *Phys. Rev. Letters* **5**, 550 (1960).
37. T. B. Bateman, H. J. McSkimin, and J. M. Whalen, *J. Appl. Phys.* **30**, 544 (1959).
38. A. L. McWhorter, *J. Appl. Phys.* **34**, 235 (1963).
39. D. T. F. Marple, *J. Appl. Phys.* **35**, 1241 (1964).
40. R. Braunstein, J. I. Pankove, and H. Nelson, *Appl. Phys. Letters* **3**, 31 (1963).

## APPENDIX I

### OPTICAL DOUBLE-PHOTON ABSORPTION IN CJS

## Optical Double-Photon Absorption in CdS†

R. BRAUNSTEIN AND N. OCKMAN  
RCA Laboratories, Princeton, New Jersey  
(Received 6 December 1963)

Observations have been made of the two-photon excitation of an electron from the valence to the conduction band in CdS ( $E_g = 2.5$  eV) using a pulsed ruby laser ( $\hbar\omega = 1.78$  eV). The radiative recombination emission from exciton and impurity levels subsequent to the simultaneous absorption of two quanta of  $\hbar\omega = 1.78$  eV was observed as a function of laser intensity and compared to the emission excited by single-quanta absorption for photons of  $\hbar\omega > E_g$ . It was found that the intensity of the recombination radiation is proportional to  $I_0^n$  for single-quanta excitation and  $I_0^{2n}$  for double-quanta excitation, where  $I_0$  is the excitation intensity and  $n$  is a constant which differs for different groups of emission lines. The observed cross section for double-quanta excitation is compared with theory utilizing the band parameters of CdS.

### I. INTRODUCTION

AN intrinsic semiconductor normally does not exhibit any optical absorption capable of producing electron-hole pairs for photon energies less than the energy gap. This is true for the light intensities employed in conventional optical absorption experiments. However, for sufficiently high incident intensities of photons whose energy is less than the band gap, the multiple-photon excitation of a valence electron to the conduction band can take place and consequently in principle, a perfectly transparent semiconductor does not exist! This type of transition involves virtual states and does not require the presence of impurity levels within the forbidden gap. In the present work,<sup>1</sup> a study has been made of the creation of electron-hole pairs in CdS by the simultaneous absorption of two photons produced by a focused ruby laser whose photon energy ( $\hbar\omega = 1.78$  eV) is considerably less than the CdS band gap ( $E_g = 2.5$  eV). The absorption was detected by observing the subsequent recombination emission produced in the region between 4900 and 5500 Å. The experimental results are compared with a theory which takes the band structure into account.

The advent of intense monochromatic sources of radiation by means of optical masers has made it experimentally feasible to observe a number of intensity-dependent optical interactions in matter which involve two or more photons. Harmonic generation<sup>2-7</sup> and optical mixing,<sup>8,9</sup> in which two photons of the same or

nearly the same frequency combine in a solid to produce a third photon, have been extensively studied. The observation of the above interactions in appropriate solids depends intimately upon the coherence of the incident light; in contrast double-photon absorption can in principle be observed with a conventional intense incoherent-light source. Since double-photon excitation depends upon the square of the incident intensity, this intrinsic absorption process is to be considered whenever a solid is irradiated with an intense light source of photon energies greater than half the band gap.

CdS was selected for the present study of double-photon absorption primarily because the single-photon absorption process has been extensively studied in this substance and it is consequently possible to compare double- and single-photon absorption on the same crystal. In addition, one can utilize the band-structure parameters determined from single-photon absorption measurements to estimate the double-photon absorption coefficients. We believe that this is the first observation of a simultaneous two-photon transition between valence and conduction bands in a semiconductor. Previously, two-photon absorption has been observed between broad bands in  $(\text{CaF}_2:\text{Eu}^{2+})^2$  and in several polycyclic, aromatic, molecular crystals,<sup>9,10</sup> as well as between discrete atomic levels in Cs vapor.<sup>11</sup> Recently, intensity-induced optical absorption has also been observed in a number of liquids.<sup>12</sup>

### II. CALCULATION OF TWO-PHOTON ABSORPTION

The general theory for two-photon absorption was first given by Göppert-Mayer.<sup>13</sup> The absorption coefficient for two-photon excitation of an electron from the valence to the conduction band in terms of the band structure parameters in a semiconductor has been

† Supported as part of Project DEFENDER under the joint sponsorship of the Advanced Research Projects Agency, the Office of Naval Research, U. S. Navy, the U. S. Department of Defense and RCA Laboratories, Princeton, New Jersey.

<sup>1</sup> A preliminary report of this work was presented at a meeting of the American Physical Society, 1963 [Bull. Am. Phys. Soc. 8, 30 (1963)].

<sup>2</sup> P. A. Franken, A. E. Hill, C. W. Peters, and G. Weinreich, Phys. Rev. Letters 7, 118 (1961).

<sup>3</sup> M. Bass, P. A. Franken, A. E. Hill, C. W. Peters, and G. Weinreich, Phys. Rev. Letters 8, 18 (1962).

<sup>4</sup> J. A. Giordmaine, Phys. Rev. Letters 8, 19 (1962).

<sup>5</sup> P. D. Maker, R. W. Terhune, M. Nisenoff, and C. M. Savage, Phys. Rev. Letters 8, 21 (1962).

<sup>6</sup> R. W. Terhune, P. D. Maker, and C. M. Savage, Phys. Rev. Letters 8, 404 (1962).

<sup>7</sup> A. Savage and R. C. Miller, Appl. Opt. 1, 661 (1962).

<sup>8</sup> W. Kaiser and C. G. B. Garrett, Phys. Rev. Letters 7, 229 (1961).

<sup>9</sup> L. Peticolas, J. P. Goldsborough, and K. E. Rieckhoff, Phys. Rev. Letters 10, 43 (1963).

<sup>10</sup> S. Singh and B. P. Stoicheff, J. Chem. Phys. 38, 2032 (1963).

<sup>11</sup> I. D. Abella, Phys. Rev. Letters 9, 453 (1962).

<sup>12</sup> J. A. Giordmaine and J. A. Howe, Phys. Rev. Letters 11, 207 (1963).

<sup>13</sup> M. Göppert-Mayer, Ann. Phys. (Paris) 9, 273 (1931).

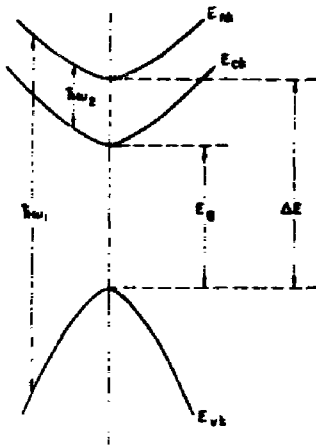


FIG. 1. Schematic diagram of band structure model used to calculate double-photon absorption.

derived by Braunstein<sup>14</sup> and extended by Loudon<sup>15</sup> to take into account the effect of excitons on the absorption coefficient close to the band edge. Two-photon excitation of impurity levels in a crystal has been considered by Kleinman.<sup>16</sup> The theory for photoelectric emission from a metal surface by two-photon absorption has been considered by Smith.<sup>17</sup> For continuity of discussion and comparison of the present experiments with theory, the band-to-band calculations for allowed transitions<sup>14</sup> will be rederived and the calculations extended to the case of forbidden transitions.

For simplicity, consider a solid whose band structure consists of a valence and two conduction bands with extrema at  $\mathbf{k}=0$ ; a schematic diagram of this model is shown in Fig. 1. If two monochromatic beams of energies  $\hbar\omega_1$  and  $\hbar\omega_2$  both less than the band gap but whose sum is greater than the gap are incident upon such a solid, the transition probability per unit time for an electron to be excited from an initial valence-band state  $\mathbf{k}$  to a final conduction-band state  $\mathbf{k}$  by simultaneously absorbing two photons is given by

$$p_{\mathbf{k},c\mathbf{k}} = \frac{2\pi}{\hbar} \left| \frac{H_{n\mathbf{k}}H_{n\mathbf{k}}}{[\Delta E + E_{n\mathbf{k}} + E_{\mathbf{k}} - \hbar\omega_1]} + \frac{H_{n\mathbf{k}}H_{n\mathbf{k}}}{[\Delta E + E_{n\mathbf{k}} + E_{\mathbf{k}} - \hbar\omega_2]} \right|^2 \times \delta(E_g + E_{c\mathbf{k}} + E_{\mathbf{k}} - \hbar\omega_1 - \hbar\omega_2), \quad (1)$$

where  $H_{n\mathbf{k}}$  and  $H_{n\mathbf{k}}$  are the optical matrix elements which couple the valence band and conduction band, respectively, to an intermediate state  $n$ .  $E_g$  is the separation of the valence and lower conduction bands at  $\mathbf{k}=0$ ,  $\Delta E$  is the separation between the valence- and intermediate-band extrema and  $E_{c\mathbf{k}}$ ,  $E_{n\mathbf{k}}$ , and  $E_{\mathbf{k}}$  are the

energies in the conduction band, intermediate band, and valence band, respectively, as measured from their extrema. In the above expression only transitions between states with the same  $\mathbf{k}$  are considered; i.e., vertical transitions, and consequently, the finite momentum of the photon was neglected. If one includes the fact that the optical matrix elements do not vanish for arbitrarily small photon wave vectors, one could use a two-band model for the calculation. In the present calculation, we have considered only one virtual state, while in fact it is usually necessary to sum over all possible intermediate states. The justification for this procedure is that the dominant contribution to the transition probability results from intermediate states which are closest to the final conduction band.

The absorption coefficient  $K_1$  for photon  $\hbar\omega_1$  when  $\hbar\omega_1$  and  $\hbar\omega_2$  are simultaneously present, may be simply related to the number of  $\hbar\omega_1$  photons absorbed per unit time per unit volume and is given by

$$K_1 = -\frac{2\pi}{c} \frac{1}{N_1} \frac{\partial N_1}{\partial t} = +\frac{2\pi}{cN_1} \sum_{\mathbf{k}} p_{\mathbf{k},c\mathbf{k}}, \quad (2)$$

where  $n$  is the index of refraction,  $c$  the velocity of light and  $N_1$  the density of photons  $\hbar\omega_1$ . The factor of two is included in the absorption coefficient to account for the two-electron spin orientations. We shall assume that there is very little spatial variation of the beam within the medium, i.e., all absorption processes are small.

By combining Eqs. (1) and (2), the absorption coefficient is given by

$$K_1 = \frac{16\pi^2 n \hbar c^4}{c m^2 \omega_1 \omega_2} \int \frac{d^3k}{(2\pi)^3} \left[ \frac{P_{n\mathbf{k}}^1 P_{n\mathbf{k}}^2}{[\Delta E + E_{n\mathbf{k}} + E_{\mathbf{k}} - \hbar\omega_1]} + \frac{P_{n\mathbf{k}}^2 P_{n\mathbf{k}}^1}{[\Delta E + E_{n\mathbf{k}} + E_{\mathbf{k}} - \hbar\omega_2]} \right]^2 \times \delta(E_g + E_{c\mathbf{k}} + E_{\mathbf{k}} - \hbar\omega_1 - \hbar\omega_2), \quad (3)$$

where the conventional optical matrix elements<sup>14</sup> have been used.  $P_{n\mathbf{k}}^1$  and  $P_{n\mathbf{k}}^2$  are the appropriate momentum matrix elements with superscripts 1 and 2 indicating their components in the directions of polarization of photons  $\hbar\omega_1$  and  $\hbar\omega_2$ , respectively.

To obtain explicit expressions of  $K_1$  for a given solid, it is necessary to have some knowledge of the momentum matrix elements as well as the  $\mathbf{k}$  dependence of  $E_{n\mathbf{k}}$ ,  $E_{c\mathbf{k}}$ , and  $E_{\mathbf{k}}$ . If the transitions are allowed, i.e., the coupling is between bands of opposite parity,  $|P_{n\mathbf{k}}^1|^2$  and  $|P_{n\mathbf{k}}^2|^2$  can be taken as constants near the band edges as a first approximation and are given in terms of the  $f$  value for the transition by:

$$|P_{c\mathbf{k}}^j|^2 = m \hbar \omega_{c\mathbf{k}} f_{c\mathbf{k}} / 2. \quad (4)$$

<sup>14</sup> R. Braunstein, *Phys. Rev.* **125**, 475 (1962).

<sup>15</sup> R. Loudon, *Proc. Phys. Soc. (London)* **80**, 952 (1962).

<sup>16</sup> D. A. Kleinman, *Phys. Rev.* **125**, 87 (1962).

<sup>17</sup> R. L. Smith, *Phys. Rev.* **128**, 2225 (1962).

<sup>18</sup> W. Heitler, *The Quantum Theory of Radiation* (Oxford University Press, New York, 1954), 2nd ed.

## OPTICAL DOUBLE-PHOTON ABSORPTION IN CDS

If the transitions are forbidden, i.e., between bands of the same parity, one may assume that the momentum matrix elements are proportional to  $\mathbf{k}_i$  of the initial state:

$$|P_{if}|^2 = (m/m_T)^2 \hbar^2 (\mathbf{e}_p \cdot \mathbf{k}_i)^2, \quad (5)$$

where  $m_T$  is an effective mass for the transition and  $\mathbf{e}_p$  represents a unit vector for the photon polarization.<sup>19</sup> We shall assume that the energy bands are spherical and parabolic and consequently are given by

$$E_{v1} = \alpha_v \hbar^2 \mathbf{k}^2 / 2m, \quad E_{v2} = \alpha_v \hbar^2 \mathbf{k}^2 / 2m, \quad E_{c1} = \alpha_c \hbar^2 \mathbf{k}^2 / 2m, \quad (6)$$

where the  $\alpha$ 's are the inverse effective-mass ratios.

There are three types of double-photon transitions to be considered depending upon the symmetries of the valence, conduction, and virtual-conduction bands. These may be defined as "allowed-allowed," "forbidden-allowed," and "forbidden-forbidden" transitions; the designations following from the appropriate matrix elements involved in the transitions. Substituting expressions, (4), (5), and (6) into Eq. (3) and performing the integrations, we obtain explicit expressions for the three possible types of transitions:

"allowed-allowed";

$$K_1 = \frac{2^{3/2} \pi n e^4 N_2 \omega_{v1} \omega_{v2} f_{v1} f_{v2}}{c m^2 (\alpha_c + \alpha_v)^2 \hbar^2 \omega_1 \omega_2} \left[ \frac{A^{1/2}}{B} + \frac{A^{1/2}}{C} \right], \quad (7)$$

"allowed-forbidden";

$$K_1 = \frac{2^{7/2} \pi n e^4 N_2 \omega_{v1} f_{v1}}{3c (m_T)^2 (\alpha_c + \alpha_v)^{5/2} \hbar \omega_1 \omega_2} \left[ \frac{A^{3/2}}{B} + \frac{A^{3/2}}{C} \right], \quad (8)$$

"forbidden-forbidden";

$$K_1 = \frac{2^{11/2} \pi n e^4 m^{7/2} N_2}{9c (m_T)^4 (\alpha_c + \alpha_v)^{7/2} \hbar^3 \omega_1 \omega_2} \left[ \frac{A^{5/2}}{B} + \frac{A^{5/2}}{C} \right], \quad (9)$$

where

$$\begin{aligned} A &= \hbar \omega_1 + \hbar \omega_2 - E_g, \\ B &= \left[ \Delta E + \left( \frac{\alpha_v + \alpha_v}{\alpha_c + \alpha_v} \right) (\hbar \omega_1 + \hbar \omega_2 - E_g) - \hbar \omega_1 \right]^2, \\ C &= \left[ \Delta E + \left( \frac{\alpha_v + \alpha_v}{\alpha_c + \alpha_v} \right) (\hbar \omega_1 + \hbar \omega_2 - E_g) - \hbar \omega_2 \right]^2. \end{aligned} \quad (10)$$

For the allowed-forbidden transition, it was assumed that the transition from the valence band to the intermediate state was allowed and that from the intermediate state to the conduction band was forbidden. In cases where the reverse is true, there will be a similar expression as Eq. (8) with  $\omega_{v1}$  replaced by  $\omega_{v2}$  and  $f_{v1}$

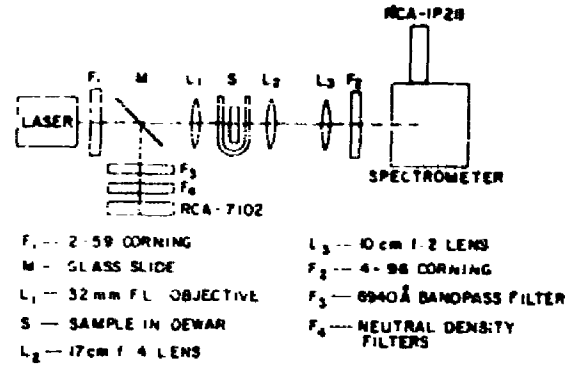


FIG. 2. Experimental arrangement for exciting double-photon absorption in CDS and observing the resulting radiative recombination. The outputs of the photomultipliers were fed directly into a dual-beam oscilloscope for comparison of the laser and fluorescence signals.

replaced by  $f_{v2}$ . In arriving at the above expressions, we have replaced the square of the sum of the matrix elements in Eq. (3) by the sum of squares which is equivalent to assuming that one is dealing with incoherent photons, since we are initially considering that the two photons  $\hbar \omega_1$  and  $\hbar \omega_2$  are produced by different sources. However, in the present experiments where the photons are of the same frequency and are derived from the same coherent source, the cross products of the matrix elements will make a small contribution to the transition probabilities. The double-photon absorption process employing a broad-band incoherent source of radiation can also be calculated from the above expressions by integrating over the spectral distribution below the band gap.

It is seen from Eqs. (7), (8), (9), and (10) that the absorption coefficient for photons  $\hbar \omega_1$  is a function of the density  $N_2$  of photons  $\hbar \omega_2$  simultaneously present in the solid. The intensity-dependent absorption edges increase as some power of the photon energy depending upon the symmetries of the bands with a threshold at  $\hbar \omega_1 + \hbar \omega_2 = E_g$ . As a consequence of these characteristics, there are a number of different types of experiments which may be performed in order to detect the resultant electron-hole pairs created by two-photon absorption. These include the direct measurement of the intensity-dependent absorption, or the observation of photoconductivity, or fluorescence produced by irradiating a solid with photons of the same or different energies, both of which are less than the energy gap but whose sum is greater than the energy gap. For experimental convenience, the double-photon absorption at  $\hbar \omega = 1.78$  eV was detected by observing the subsequent recombination emission in the region between 4900 and 5500 Å produced by the created pairs.

## III. EXPERIMENTAL

The fluorescence spectrum was measured for a number of CDS crystals excited by a focused ruby laser whose

<sup>19</sup> J. Bardeen, F. J. Blatt, and L. H. Hall, in *Proceedings of the Conference on Photoconductivity, Atlantic City, November 4-6, 1954*, edited by G. H. Breckenridge, B. R. Russell, and E. F. Hahn (John Wiley & Sons, Inc., New York, 1956), p. 146.

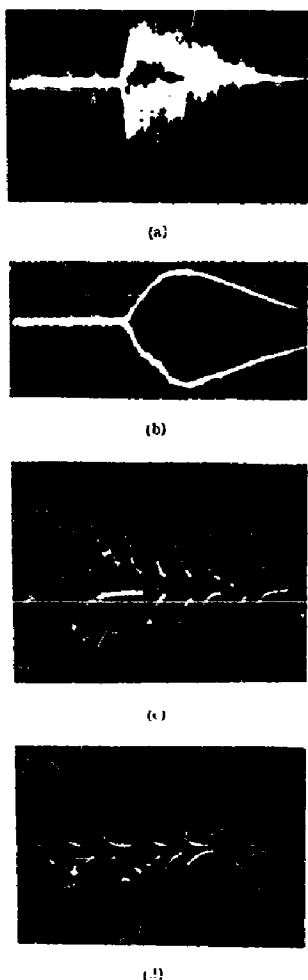


FIG. 3. Correlation between the emission of CdS at 123°K and the exciting ruby laser. In each figure the upper trace is the laser signal and the lower trace is the fluorescence signal; (a) emission at 4990 Å, horizontal sweep 100  $\mu$ sec/cm; (b) same as (a) except for a larger time constant in detecting circuits; (c) same as for (a) but with horizontal sweep of 5  $\mu$ sec/cm; (d) emission at 5100 Å same time constant as (a) but with horizontal sweep of 5  $\mu$ sec/cm. Note the perfect time correlation in (c) for exciton recombination and the slightly delayed electron-impurity emission in (d).

photon energy  $\hbar\omega = 1.78$  eV is less than the energy gap  $E_g = 2.5$  eV, as well as by the conventional use of the 3660 Å Hg line, whose photon energy is greater than the energy gap. The spectral distribution as well as the intensity of the emission was determined as a function of incident intensity for both types of excitation. The spectra shown in this paper were for a typical undoped crystal of dimensions 10 mm  $\times$  8 mm  $\times$  1.78 mm grown at the RCA Laboratories; similar results were obtained using undoped crystals supplied from other sources.

A schematic diagram of the experimental arrangement for observing the emission from crystals using the focused ruby laser is shown in Fig. 2. The ruby rod was 3 in. long and  $\frac{1}{4}$  in. in diam with parallel ends coated with multilayer dielectric films giving 100% reflectivity on one face and 50% reflectivity on the other for the 6943 Å line. The ruby was mounted in a conventional laser head and was optically pumped by a helical GE FT-524 flash lamp. Operated at room temperature, this laser produced approximately 0.1 joules of output power which is equivalent to  $4 \times 10^{17}$  photons per flash. When focused onto an area of  $10^{-2}$  cm<sup>2</sup> of the sample, the

photon density was  $3 \times 10^{19}$ /cm<sup>2</sup>; larger energy densities produced by sharper focusing resulted in sample damage. The crystals were mounted in a Dewar which contained liquid nitrogen for the low temperature runs. The sample temperature was measured by an iron-constantan thermocouple cemented directly to the crystal. The spectra were measured by a Perkin-Elmer model 12C Spectrometer using a CaF<sub>2</sub> prism and utilizing an RCA 1P28 photomultiplier as a detector. The laser beam was monitored by reflecting part of the beam into an RCA 7102 photomultiplier. Filters  $F_1$  and  $F_2$  eliminated most of the xenon flash lamp radiation while  $F_2$  attenuated the laser emission; their position in the optical chain is shown in Fig. 2.

In the studies of the emission excited by Hg excitation, a Bausch and Lomb monochromator using a 600 lines/mm grating was used. The HBO-500 mercury source was focused by a large aperture lens or mirror onto the crystals immersed in liquid nitrogen. The radiation, which was emitted from the same face of the crystal which received the excitation radiation was focused onto the monochromator slit after passing through appropriate filters. A Corning 7-54 filter and 10 cm of CuSO<sub>4</sub> solution isolated the 3660 Å Hg line. The emitted radiation was detected by an RCA 7265 photomultiplier whose output was fed to a recorder via a Vibron electrometer.

#### IV. RESULTS

The experimental results involve a comparison of the fluorescence spectra of CdS as excited by the 3660 Å Hg line with that excited by the 6943 Å ruby laser line. The emission spectrum was studied in the 4900- to 5500-Å region for both means of excitation since it is in this spectral region that previous single-quanta excited-fluorescence spectra have been extensively studied. The "green emission" bands in the region between 5100-5400 Å at 77°K have been previously identified as due to recombination of a free electron with a trapped hole,<sup>20-22</sup> while the so-called "blue emission" bands appearing at shorter wavelengths are presumably due to the recombination of free electron-hole pairs via an exciton state.<sup>21-22</sup> The emission was studied as a function of wavelength, time, polarization, and excitation intensity for the ruby excitation; and as a function of wavelength and excitation intensity for the Hg source.

##### A. Double-Photon Excited Emission

The correlation between the emission of CdS at 123°K and that of the exciting ruby laser is shown in Fig. 3. The detected output of the laser and the CdS emission were both displayed on separate channels of a Tektronix

<sup>20</sup> G. Diemer, G. J. van Gorp, and H. J. G. Meyer, *Physica* 23, 987 (1957).

<sup>21</sup> G. Diemer and A. J. Van der Houven van Oord, *Physica* 24, 707 (1958).

<sup>22</sup> R. J. Collins, *J. Appl. Phys.* 30, 1135 (1959).

<sup>23</sup> D. G. Thomas and J. J. Hopfield, *Phys. Rev.* 116, 573 (1959).

## OPTICAL DOUBLE-PHOTON ABSORPTION IN CdS

502 dual-beam oscilloscope. Figure 3(a) shows the partially resolved laser and emission spikes where it is seen that on the average the relative intensities are correlated with each other. This observation is further illustrated in Fig. 3(b) where a larger time constant in the detector circuits averaged the spikes. A time-expanded display of the laser and emission spikes is shown in Figs. 3(c) and 3(d). It should be noted that at 4990 Å, the region of exciton recombination, there is a perfect time correlation between exciton and emission spikes. In the region of electron-trapped hole recombination at 5100–5400 Å, there appears to be a time delay of several microseconds between the emission and the excitation spikes. The usefulness of using laser spikes for studying the kinetics of emission processes is clearly indicated by these results. Although there is no apparent correlation of the intensity of the excitation and emission spikes in the time expanded traces in Figs. 3(c) and 3(d), the correlation of the envelope of the laser and emission spikes previously indicated in Figs. 3(a) and 3(b) justifies the use of the envelope maxima as a measure of relative signal intensities. The lack of intensity correlation in the time expanded scale may be due to the detailed kinetics of the respective recombination processes.

The unpolarized and polarized emission spectra of a CdS crystal at 300°K excited by the laser is shown in Fig. 4. Previously, the CdS emission had only been observed at room temperature in a limited number of cases for excitation by photons greater than the energy gap.<sup>24</sup> The intensity of the emission varied from sample to sample for a given incident laser intensity; these

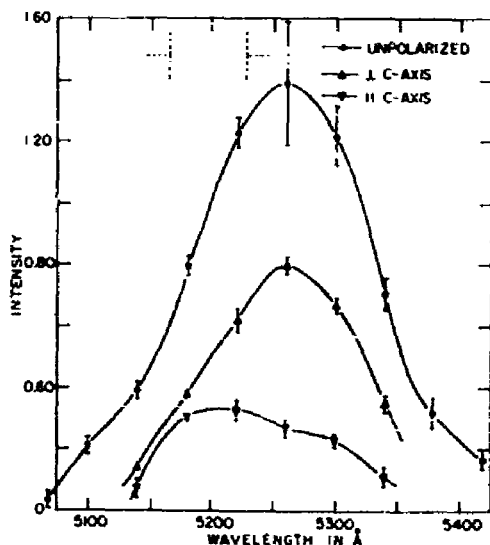


FIG. 4. Emission from CdS at 300°K excited by a focused ruby laser. The laser output was 0.17 J focused into a  $10^{-2}$  cm<sup>2</sup> area of the crystal.

<sup>24</sup> B. A. Kulp, R. M. Detweiler, and W. A. Anders, Phys. Rev. 131, 2036 (1963).

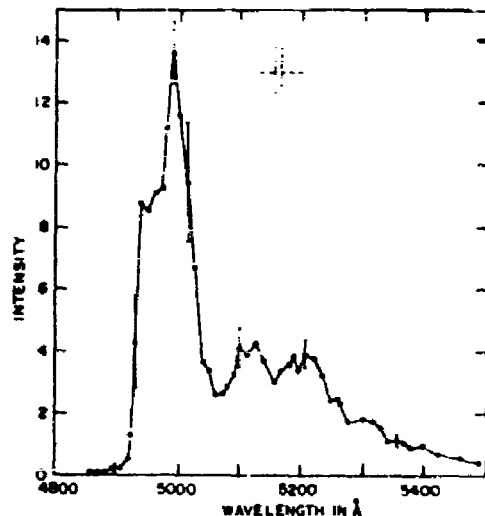


FIG. 5. Emission from CdS at 123°K excited by a ruby laser with 0.15 J focused into a  $10^{-2}$  cm<sup>2</sup> area of the sample.

differences in quantum efficiencies are not surprising in the light of previous work on CdS. It is seen in Fig. 4 that the emitted radiation is polarized, the intensity perpendicular to the *c* axis is about three times that parallel to the axis. The recombination radiation was observed to follow the power law  $I \propto I_0^{2.10 \pm 0.2}$  where *I* is the emission intensity and *I*<sub>0</sub> is the laser intensity. In obtaining these measurements, *I*<sub>0</sub> was varied by inserting neutral-density filters between the laser and the focusing lens. Each data point in Fig. 4 is the average of between two and five successive observations; the error lines indicate maximum deviations from the average. Since the laser intensity varied slightly from flash to flash, the observed emission intensities were normalized to the same laser intensity for all the recorded spectra. In the normalization procedure for this spectrum and all subsequent spectra reported in this work, the appropriate empirically determined power law relating the intensity of the emission to excitation was employed.

The above measurements were also performed at low temperatures where it was possible to observe fluorescence by ruby-laser excitation as well as by single-quanta Hg excitation for comparison. The observed unpolarized emission spectra at a temperature of 123°K is shown in Fig. 5. The rather large errors indicated in this spectrum make it difficult to ascribe some of the wiggles as due to real structure. However, successive runs enabled one to identify the major lines in this spectrum with the structure observed by using greater than band gap light; the line positions agree with those reported in the literature.<sup>22,21</sup> The emission shown in Fig. 5 was found to be polarized with the component perpendicular to *c* axis being six times greater than the component parallel to the *c* axis.

Two groups of lines in the above spectrum exhibit

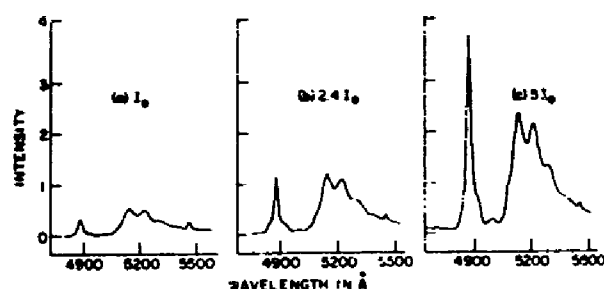


FIG. 6. Fluorescence spectra from CdS at 77°K as a function of incident intensity excited by the 3660-Å line of Hg.

different power laws relating the fluorescence to excitation intensity. Namely, the intensity of the lines between 4900 and 5050 Å varied as  $I \propto I_0^{2.4 \pm 0.2}$  while for the lines between 5050 and 5400 Å the relationship is  $I \propto I_0^{1.4 \pm 0.1}$ . The emission obeyed these power laws over a range of  $I_0$  of  $10^2$ . The significance of the difference will be discussed after similar relationships for the single-quanta excitation are presented.

### B. Single-Photon Excitation

The unpolarized emission spectra at 77°K excited by the 3660-Å Hg line is shown in Fig. 6 for three different excitation intensities. There is a marked similarity between this single-photon excited spectra and the double-photon ruby laser excited spectra shown in Fig. 5. In general, the wavelengths observed for both means of excitation agree within experimental error. The major differences between the two spectra are with respect to the relative intensities of the various groups of lines. The failure of the intense 4875-Å band to appear in the laser-excited spectra is probably due to self-absorption in the sample since the emission was observed from the side opposite the incident laser beam. Double-photon absorption takes place essentially throughout the bulk of the solid and since the single-quanta absorption coefficient of CdS at 4875 Å is very large, the excited radiation at this wavelength will be self-absorbed. In contrast, for the case of the Hg excitation, the emission is collected from the same face as the incident excitation and so is generated close to the surface and can exit from the sample. The relative weakness of the 4940-, 4960-, and 4990-Å lines in the single-photon compared to the double-photon excited spectra is most likely due to the much smaller exciting intensity of the Hg source, relative to the effective double-photon pumping. A more detailed discussion of this point will be given later.

The different intensity law followed by the exciton recombination and the electron-trapped hole recombination is dramatically shown in Fig. 6 where it is seen that at low intensities the line at 4875 Å is weaker than the "green group" of lines at 5000–5400 Å while at high intensities it becomes larger than the latter group. The exciton lines at 4900–5000 Å follow the law  $I \propto I_0^{1.4 \pm 0.1}$  while the "green" lines follow the relationship

$I \propto I_0^{2.4 \pm 0.2}$ . This is to be contrasted with the power laws  $I \propto I_0^{2.4 \pm 0.2}$  and  $I \propto I_0^{1.4 \pm 0.1}$  for the corresponding lines in the double-photon excited spectra. The various power laws are shown in Fig. 7. The different intensity dependence for the exciton and electron-hole recombination is consistent with the previous observation by Diemer<sup>21</sup> which was used by him to identify the respective recombination processes.

The quantum efficiency was measured at 77°K for the crystal used to obtain the spectra in Figs. 4 and 5 and was found to be approximately 0.1% for the 4990-Å line. The quantum efficiency is here defined as the ratio of the rate of emission to excitation since the intensity law for the 4990-Å line is approximately linear. The fluorescence yield for the front surface Hg excitation was found to be markedly dependent upon the surface treatment, while the double-photon yield was independent of this surface treatment. The above value of quantum efficiency was obtained for a well etched or cleaved surface.

We may summarize the experimental results shown in Figs. 4, 5, 6, and 7 by the observation that in general the spectra produced by both types of excitation are essentially similar except for differences in the emission intensity as a function of excitation intensity. The fact that the intensity of the emission spectra for the ruby-laser excitation increases within experimental error as the square of the corresponding Hg excitation over several decades for equivalent groups of lines strongly suggests that the former are due to double-photon absorption while the latter correspond to single-photon absorption.

### C. Auxiliary Measurements

There are two alternate excitation mechanisms which could produce the observed fluorescence other than the

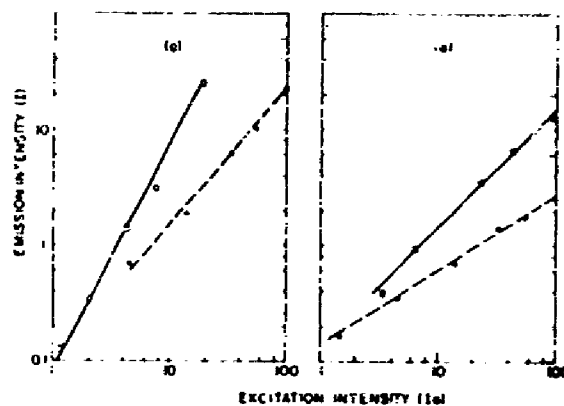


FIG. 7. Relative intensity of emission from CdS as a function of excitation intensity for both the Hg 3660 Å line and the ruby laser. In both figures the solid lines refer to laser excitation with crystal at 123°K while the dashed lines refer to Hg excitation at 77°K. (a) Emission of exciton recombination line at 4990 Å; (b) emission of electron impurity recombination line at 5120 Å. Note that the emission follows a power law of the form  $I \propto I_0^n$  where  $n$  for laser excitation is twice that for Hg excitation for each line.

creation of free electron-hole pairs by the simultaneous absorption of two laser photons via a virtual intermediate state. One is the self-absorption in the sample of a generated second harmonic  $2h\nu = 2 \times 1.78 \text{ eV} > E_g = 2.5 \text{ eV}$  and the consequent creation of an electron-hole pair by a final single-photon process. The second is two-photon absorption via an impurity state within the forbidden gap. In order to rule out these processes in the present experiments, the following auxiliary measurements were made.

As a consequence of the symmetry of the space group of CdS, (6 mm) one can easily show that if the laser beam is incident along the  $c$  axis no second harmonic should be generated. Consequently, if the observed emission depends on the absorption of second harmonic photons, there should be no emission for the above geometry. To check this point a CdS sample was cut from the same boule as was a previously studied crystal such that its  $c$  axis was perpendicular to its faces enabling the incident laser beam to be parallel to the  $c$  axis. At 300°K, this crystal exhibited the same intensity of recombination emission as the crystal whose  $c$  axis was perpendicular to the laser beam for the same excitation intensities. Hence one can disqualify the absorption of second harmonics of ruby as the fluorescence-excitation mechanism. It should be noted that the absence of second-harmonic generation applies strictly speaking only if the incident beam is parallel to the  $c$  axis. However the harmonic intensity for the convergent excitation employed would be too weak to be of any importance.

It has previously been shown that emission in CdS at 2.5 eV as well as at lower energies can be excited by photons having energies not exceeding 1.75 eV.<sup>25,26</sup> These results were explained by considering a two-step optical-excitation process involving excited states of Cu impurity levels within the forbidden gap. In this process, a photon produces excitation to an excited level that has a reasonably long lifetime and then a second photon completes the excitation and is to be distinguished from double-photon absorption discussed above which involves the simultaneous absorption of two photons and is an intrinsic property of the solid. We found in agreement with the previous work<sup>25</sup> that tungsten excitation of our CdS crystals by photons having energies between 1.1 and 1.8 eV led to the same fluorescence as was observed with Hg excitation. However, we did not observe this emission for tungsten excitation for photon energies of 1.78 eV (the same as the laser) with a half-width of  $\sim 0.02 \text{ eV}$ . These results are contrary to the excitation curves obtained in the previous work<sup>26</sup> which substantiated the proposed two photon excitation process via

<sup>25</sup> R. E. Halsted, E. F. Apple, J. S. Prener, *Phys. Rev. Letters* **2**, 420 (1959).

<sup>26</sup> R. E. Halsted, E. F. Apple, J. S. Prener, and W. W. Piper, in *Proceedings of the International Conference on Semiconductor Physics, Prague, 1960* (Czechoslovakian Academy of Science, Prague, 1961).

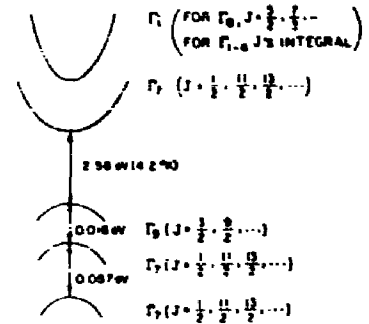


FIG. 8. The energy band structure of CdS at  $k=0$  with the associated band symmetries.

copper impurity levels. The intensities of emission for different crystals at 123°K obey the relationship  $I \propto I_0^n$  with  $n$  constant for a given line over a number of decades for the laser excitation. It seems likely that a mechanism involving the replenishment of electrons from the initial copper level by the absorption of a second photon promoting electrons from the valence band to this copper level would lead to saturation effects over the range of excitation intensities of our experiments. The difference between our results for tungsten excitation and the previous work may lie in differences between our crystals and those employed in the above work.

## V. DISCUSSION

We believe that the recombination radiation observed from CdS when excited by a ruby laser is a consequence of electron-hole pair creation by the simultaneous absorption of two red photons via a virtual intermediate state. The strongest experimental evidence for this conclusion follows from the detailed comparison of the fluorescence spectra as excited by the 3660-Å line of Hg, whose energy is greater than the band gap, with that produced by the 6943-Å laser line which is less than the band gap. The spectral distribution of the emission for both types of excitation are essentially similar, except for differences in the intensity dependence of the emission as a function of excitation intensity. The observed approximate quadratic dependency of the emission for laser excitation as compared with excitation by photon energies greater than the gap is to be expected if double-photon absorption were operative.

We shall now compare the observed fluorescence yields with the theory for double-photon absorption as further evidence that this excitation process can account for the observed spectra. The energy bands<sup>27</sup> for CdS at  $k=0$  are shown in Fig. 8 and the corresponding selection rules for double photon absorption for electric dipole transitions at  $k=0$  are shown in Table I where the single photon selection rules were used in the individual transitions.<sup>28</sup> In the present experiment, the final state in the conduction band is at  $2 \times 1.78 \text{ eV}$ , well above  $k=0$ , and consequently it is not possible to

<sup>27</sup> Joseph L. Birman, *Phys. Rev.* **114**, 1490 (1959).

<sup>28</sup> D. S. McClure, *Solid State Physics*, edited by I. Seitz and D. Turnbull (Academic Press Inc., New York, 1959), Vol. 9, p. 432.

TABLE I. Selection rules for double-quantum absorption in CdS for electric dipole transitions at  $k=0$ .

Valence Band	Virtual Band	Conduction Band	Designation
$\Gamma_6$	$\parallel$	$\Gamma_7$	Allowed-allowed
$\Gamma_6$	$\perp$	$\Gamma_7$	Allowed-allowed
$\Gamma_6$	$f$	$\Gamma_7$	Allowed-forbidden
$\Gamma_6$	$f$	$\Gamma_7$	Forbidden-forbidden
$\Gamma_7$	$\parallel, \perp$	$\Gamma_7$	Allowed-allowed
$\Gamma_7$	$\perp$	$\Gamma_7$	Allowed-allowed
$\Gamma_7$	$f$	$\Gamma_7$	Forbidden-forbidden

scribe a definite parity to the appropriate point in the Brillouin zone. Since we are primarily interested in an order of magnitude estimate of the absorption coefficient, we shall make the somewhat oversimplified, but reasonable assumption, that the CdS band structure can be represented by a spherical and parabolic three-band model as is shown in Fig. 1.

The expressions for "allowed-allowed" and "allowed-forbidden" transitions in Eqs. (7) and (8) will only be considered, since Eq. (9) for the "forbidden-forbidden" transitions yields much smaller values than are actually observed. In the above expressions,  $\omega_1 = \omega_2 = 4 \times 10^{14}$  sec<sup>-1</sup>,  $E_0 = 2.5$  eV,  $m_v = m$ ,  $f_{va} = f_{vc} = 1$ ,  $n = 2.6$  and  $N_2 = 2 \times 10^{13}$ /cm<sup>3</sup> for the present experiment.  $K_1$  is rather insensitive to values of  $\Delta E$  varying from 2.4 to 5.5 eV. The inverse effective-mass ratios for CdS were taken as  $\alpha_c = 5$ ,  $\alpha_v = 0.2$  and  $\alpha_n = 1$ . The first two values were obtained from optical-absorption experiments,<sup>22</sup> while the latter was assumed to be unity since the upper conduction band is expected to be a heavy mass band. Using the above values, Eqs. (7) and (8) give  $K_1 = 2 \times 10^{-4}$  cm<sup>-1</sup> for the "allowed-allowed" transition and  $4 \times 10^{-6}$  cm<sup>-1</sup> for the "allowed-forbidden" case, respectively. If we use the experimentally determined quantum efficiency of 0.1% obtained from the single-photon Hg excitation of the 4990-Å line at 77°K, the calculated double-photon absorption coefficients predict corresponding fluorescence yields per laser flash of  $8 \times 10^9$  photons and  $2 \times 10^8$  photons for the respective transitions. The measured emission of the 4990-Å line at 123°K for laser excitation was  $2 \times 10^{11}$  photons at 123°K. This value has been corrected for an estimated loss factor of  $\sim 10^3$  due to internal reflection losses in the sample and losses in coupling the output from the crystal into the spectrometer. It is seen that the observed value is in closer agreement with the calculated "allowed-allowed" rather than with the "allowed-forbidden" transitions. It was not possible to compare the room-temperature double-photon absorption signal with experiments since the inability to observe the single-photon emission at this temperature prevented the determination of the quantum efficiency.

The observation shown in Fig. 5 that the exciton emission lines are more intense relative to the electron-impurity recombination lines for double-photon laser excitation in contrast to the case for single-photon Hg

excitation shown in Fig. 6 can be understood from a consideration of the number of electron-hole pairs created by both sources. As we have seen, the exciton and impurity emission are proportional to  $I_0^{1/2}$  and  $I_0^{0.6 \pm 0.05}$ , respectively, for single-photon excitation and to  $I_0^{2/3}$  and  $I_0^{1/2}$  for double-photon absorption; therefore for a sufficiently high excitation intensity the exciton emission should exceed the impurity emission. Although the double photon absorption coefficient for the ruby is  $\sim 2 \times 10^{-4}$  cm<sup>-1</sup>, while for the Hg line the single-photon coefficient is  $\sim 10^6$  cm<sup>-1</sup>, the laser flux was  $6 \times 10^{22}$  photons/cm<sup>2</sup> sec while for the 3660-Å line of Hg it was  $10^{13}$  photons/cm<sup>2</sup> sec; consequently approximately  $10^4$  more electron hole pairs were created by the laser than the Hg source which is sufficient to explain the different relative intensities. Although the power laws for Hg and laser excitation were obtained for different effective excitation intensities, the fact that the emission due to laser excitation is consistent with double-photon absorption for two different recombination processes indicates that the power laws shown in Fig. 7 would also hold for equal effective intensities of both sources.

One may regard the calculated double-photon absorption coefficients to be in reasonable agreement with experiment in view of the approximations made in its application to CdS and the experimental errors involved in determining the absolute fluorescence yield. The use of a three-band model with spherical and parabolic energy surfaces and the neglect of coherence effects and the effect of other conduction and valence bands could lead to appreciable errors in the estimates of the double-photon absorption coefficients. In addition, the theory should only be a good approximation in the vicinity of  $k=0$ , whereas the final state for the double photon observation of 1.78-eV photons was at much greater values of  $k$ . The experimental yields may be in error by as much as a factor of 50 because of uncertainties in geometric factors which were used to calculate the yields.

The present experiment and theoretical estimates of double-photon absorption were merely intended as an order of magnitude check of this type of intrinsic absorption process. These results suggest the feasibility of performing two-beam absorption experiments employing a fixed-frequency ( $\hbar\omega_1$ ) high intensity laser and a low-intensity variable-frequency ( $\hbar\omega_2$ ) incoherent source where  $\hbar\omega_1 < E_g/2$ ,  $\hbar\omega_2 < E_g$  and  $\hbar\omega_1 + \hbar\omega_2 > E_g$ . The low-intensity source can be utilized since as we have shown previously, its absorption coefficient  $K_1$  is proportional to the intensity of the intense source. This absorption coefficient can be measured directly or effectively by the subsequent fluorescence or photoconductivity. The frequency and polarization dependence of the absorption edge can yield information about the states involved in the virtual transitions by reference to Eqs. (7), (8), and (9) and the selection rules shown in Table I.

Double-photon absorption can be of use in a number

## OPTICAL DOUBLE-PHOTON ABSORPTION IN CdS

of optical studies. In cases where single-photon transitions between levels are forbidden for electric-dipole radiation, transitions can still be made by a double-photon process. In order to study transitions to states that have large absorption coefficients by single-photon absorption, one normally requires thin samples, or one performs reflectivity experiments which can be sensitive to surface treatment. The fact that photons of energy less than the band gap can produce transitions to states of twice the energy of the incident photon can be used to study upper states by the use of thick samples since the double-photon transitions take place throughout the bulk of the material.

[*Note added in proof.* The observation of a two-quantum absorption spectrum employing a high-intensity laser and a low-intensity variable-frequency incoherent light source in an experiment of the type suggested in this paper has been performed by J. J. Hopfield, J. M. Warlock, and Kwangjai Park, Phys. Rev. Letters 11, 414 (1963) in KI.]

### ACKNOWLEDGMENT

The authors wish to acknowledge the contribution of A. B. Dreeben for the samples used in this work and are grateful to D. A. Kramer for assistance in these measurements.

## APPENDIX II

### FREQUENCY TUNING OF GaAs LASER DIODE BY UNIAXIAL STRESS

FREQUENCY TUNING OF GaAs LASER DIODE BY UNIAXIAL STRESS

Dietrich Meyerhofer and Rubin Braunstein

RCA Laboratories

Princeton, New Jersey

(Received 23 September 1965)

Now that GaAs injection laser diodes are readily available it becomes desirable to vary their frequency in a controlled manner. Such control will be necessary if diodes are to be used in technical applications requiring frequency tuning, stabilization, or modulation. The energy levels and consequently the emission frequency of a solid can be changed by uniaxial stress. Use of uniaxial stress has the advantage over other methods of changing the frequency (hydrostatic pressure,<sup>1</sup> magnetic field<sup>2</sup>) in that auxiliary equipment can be made simpler and smaller. In addition, the application of uniaxial stress to semiconductors generally splits energy levels which are degenerate in the absence of stress or under hydrostatic pressure, and so can be used as a means of identifying recombination processes.

Figure 1 shows the effect of uniaxial compression on the coherent emission of a typical lasing diode. The stress is applied perpendicularly to the junction, which is a (100) plane. The emission lines are not single resonant modes of the diode, but rather envelopes of a number of such modes. Unfortunately, samples small enough so that individual modes could be resolved were too fragile for stress measurements. Shifts of the location of the envelopes as well as "moding" from one set of envelopes to another have been observed with uniaxial stress. These changes do not necessarily vary monotonically with stress, as can be seen in Fig. 1. The maximum shift of the laser line in this diode was 20 Å or 0.25% in frequency. In some diodes the envelope curves narrowed with increasing stress, suggesting that fewer modes lased under this condition; in other

words, the coherent emission is affected both by changes in the emitting transitions and by changes in the resonant cavity, which will be somewhat different for every diode.

To eliminate the effects of cavity changes we studied the incoherent light, which should depend only on the electronic transition. The shape of this emission line was independent of the applied stress, so that the only varying quantity was the emission frequency. The change of energy (or frequency) is plotted in Fig. 2 as a function of uniaxial compressive stress for three diodes. It is clear that the three diodes, all made by solution growth but with different amounts of doping, show very different behavior; the frequency of A increases linearly with stress whereas B and C show

CONTENT ANALYSIS	
A. GaAs lasers	D. 77°K
B. frequency tuning	E/T
B. recombination process	
identification	
C. uniaxial stress	

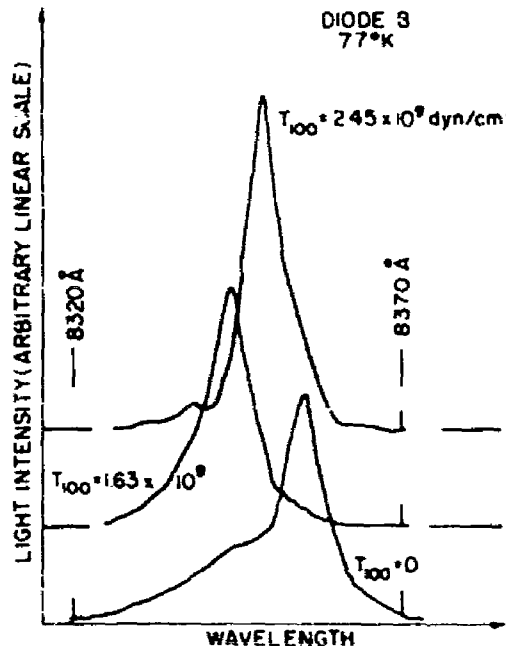


Fig. 1. Recorder trace of the coherent emission line from a GaAs diode at three different values of stress applied along the [100] direction. The curves are displaced vertically for clarity. The linewidths are due to unresolved modes (instrumental resolutions ~1 Å).

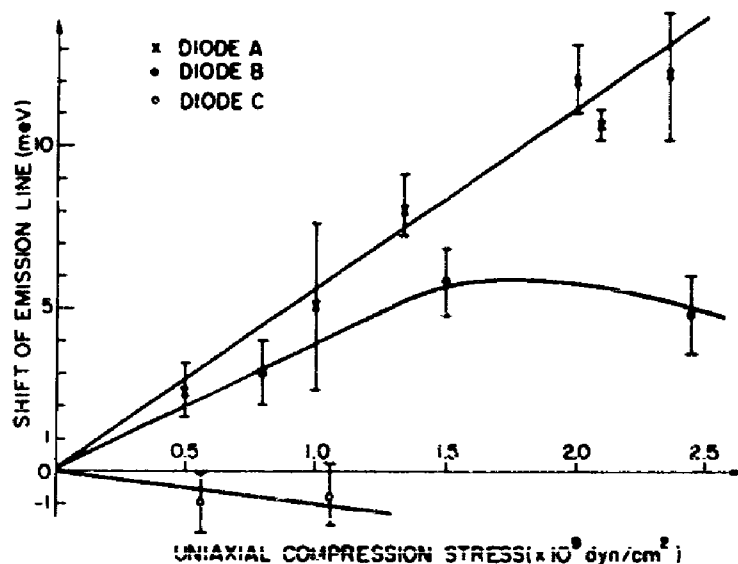


Fig. 2. Shift of the incoherent emission line from three typical GaAs diodes with uniaxial compression stress at 77°K. Each data point represents three or more measurements.

saturation and even negative changes. Other diodes made in the same way as A, B, or C do reproduce the respective curves. It should be noted that the frequency shift of diode B is the same for coherent (Fig. 1) and incoherent emission (Fig. 2).

If the emission is due to band-to-band recombination or recombination via an exciton, then one can calculate that the emission line is both shifted in its average value and split into two components due to strain. For simplicity we shall assume that the band structure of GaAs at  $k = 0$  is the same as that of Ge and use the theory developed for Ge<sup>3</sup> that predicts a linear shift of the average emission line with stress. The coefficient can be calculated from the measured effects of hydrostatic pressure on optical absorption<sup>4</sup> and emission<sup>1</sup> of GaAs, or from the effect of shear stress on the absorption.<sup>5</sup> For compression along the [100] direction the three sets of data predict a value of  $(4.0 \pm 0.9) \times 10^{-12} \text{ eV}/(\text{dyn}/\text{cm}^2)$ . The expected splitting of the line is  $\sim 0.6 \times 10^{-12} \text{ eV}/(\text{dyn}/\text{cm}^2)$ , too small to observe with the precision available.

Diode A (Fig. 2) shows the predicted linear variation of frequency with stress. The coefficient is  $(5.5 \pm 1.0) \times 10^{-12} \text{ eV}/(\text{dyn}/\text{cm}^2)$ , in agreement with the calculated value for band-to-band transitions, and consistent with the hydrostatic pressure results. The same behavior would be expected for transitions to or from impurity levels which are tightly bound to one of the bands. In contrast the

behavior of type B and C diodes can certainly not be explained by the simple model. Rather the emission appears to take place between energy levels that are more complicated. They may be shifted relative to the band edges and split in a complicated manner. A detailed interpretation of the nature of these centers will require further measurements on diodes with different dopings and stress orientations.

We have shown that uniaxial compression will shift the frequency of a GaAs laser by a substantial amount. We expect other injection lasers made from III-V compounds and alloys to show similar shifts, since the deformation potentials are expected to be the same order of magnitude. Furthermore, uniaxial stress has been shown to be a very sensitive tool for studying the electronic transitions in light-emitting diodes.

We wish to thank H. Nelson for supplying the diodes and H. Ogawa for assisting in the experimental measurements.

<sup>1</sup>J. Feinleib, S. Groves, W. Paul, and R. Zallen, *Phys. Rev.* **131**, 2070 (1963).

<sup>2</sup>F. L. Galeener, G. B. Wright, W. E. Krag, T. M. Quist, and H. J. Zeiger, *Phys. Rev. Letters* **10**, 476 (1963).

<sup>3</sup>W. H. Kleiner and L. M. Roth, *Phys. Rev. Letters* **2**, 334 (1959).

<sup>4</sup>W. Paul, *J. Appl. Phys.* **32**, 2082 (1961).

<sup>5</sup>M. D. Sturge, *Phys. Rev.* **127**, 768 (1962).

## APPENDIX III

### EFFECT OF DOPING ON THE EMISSION PEAK AND THE ABSORPTION EDGE OF GaAs

EFFECT OF DOPING ON THE EMISSION PEAK AND  
THE ABSORPTION EDGE OF GaAs

R. Braunstein, J. I. Pankove, and H. Nelson

RCA Laboratories

Princeton, New Jersey

(Received 14 June 1963)

Nathan and Burns<sup>1</sup> have shown that the fluorescence peak of zinc-doped gallium arsenide moves to lower energies as the zinc concentration increases. In the present Letter we shall show that the band-to-band radiative recombination spectrum depends

also on the donor concentration, and that this dependence might be attributed to a concentration-dependent shrinkage of the energy gap.

Figure 1 shows the energy of the emission peak and the spectral halfwidth obtained with a number of diodes at 78°K. Because the energy of the emission peak usually varies with the current through the diode,<sup>2,3</sup> all the data of Fig. 1 were taken with roughly the same current density, about 50 A/cm<sup>2</sup>. Diodes made with known tin or silicon concentrations were fabricated by zinc diffusion to produce a *p-n* junction. Hence, at the *p-n* junction, the zinc concentration was approximately the same as the donor concentration (this statement assumes that there was one free carrier per impurity regardless of its chemical nature — which is not always true<sup>4</sup>). Diodes made with a known zinc concentration were fabricated by alloying a tin dot to the *p*-type crystal.

CONTENT ANALYSIS	
A. lasers, GaAs diodes	
B. effect of doping on emission and absorption	
D. 300°K, 77°K	
E.	

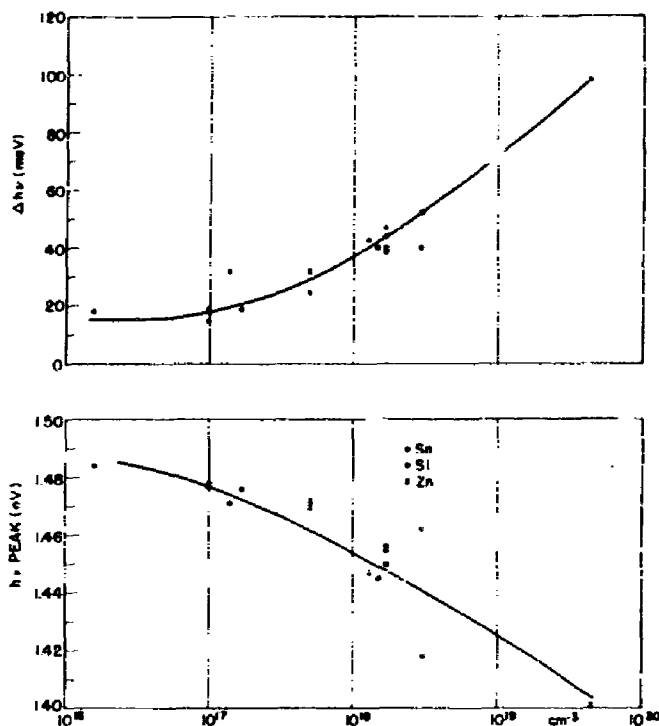


Fig. 1. Dependence of the spontaneous emission spectrum in GaAs  $p$ - $n$  junctions traversed by about  $50 \text{ A/cm}^2$  at  $78^\circ\text{K}$  on the carrier concentration. Top curve: variation of the spectral halfwidth; bottom curve: variation of the emission peak.

It is evident from Fig. 1 that the donor concentration had a profound influence on the incoherent light emitted by the  $p$ - $n$  junction: The emission peak shifted to lower energies by about 40 meV for a two-order-of-magnitude increase in donor concentration; and the line width increased by a factor of three. It is remarkable that the zinc data (alloyed junctions) follow the same trend as the data obtained with donors for incoherent operation. All the diodes obtained by diffusion showed laser action. The photon energy at coherence was lowered by about 15 meV as the donor concentration was increased by one order of magnitude.

One striking feature of the emission spectrum is that even at the highest currents most of the emission occurs at energies lower than that of the gap in pure GaAs ( $1.52 \text{ eV}$ <sup>5,6</sup>). This raises the question about the possible perturbation of impurities on the band structure of this semiconductor. In the case of germanium, it was found that a high impurity concentration caused a large shrinkage of the energy gap.<sup>7,8</sup> Reasoning by analogy we may expect a similar effect in GaAs.

Absorption spectra of heavily doped  $n$ -type,  $p$ -type, and compensated GaAs were measured at room temperature. The absorption coefficients derived from these measurements are shown in Fig. 2. The absorption edge of heavily doped  $n$ -type material<sup>9</sup> occurs at a higher energy than that of the purer material ( $n = 1 \times 10^{16} \text{ cm}^{-3}$ ); however, when one takes into account the penetration of the Fermi level into the conduction band, one finds that the conduction band edge is at a lower energy than in the case of the purer material. The absorption edge of heavily doped  $p$ -type material is shifted to lower energy as the zinc concentration increases. In the present case, at room temperature, because of the large density of state effective mass of the valence band, no correction was needed for the penetration of the Fermi level; i. e., practically all the holes were at the valence band edge. The similarity in shape of the absorption edges for pure and for  $p$ -type material suggests that one deals here with similar band-to-band transitions. The present data suggest an appreciable shrinkage of the energy gap due to heavy doping. In the compensated material with  $5 \times 10^{17} \text{ holes/cm}^3$  (the impurity concentration is

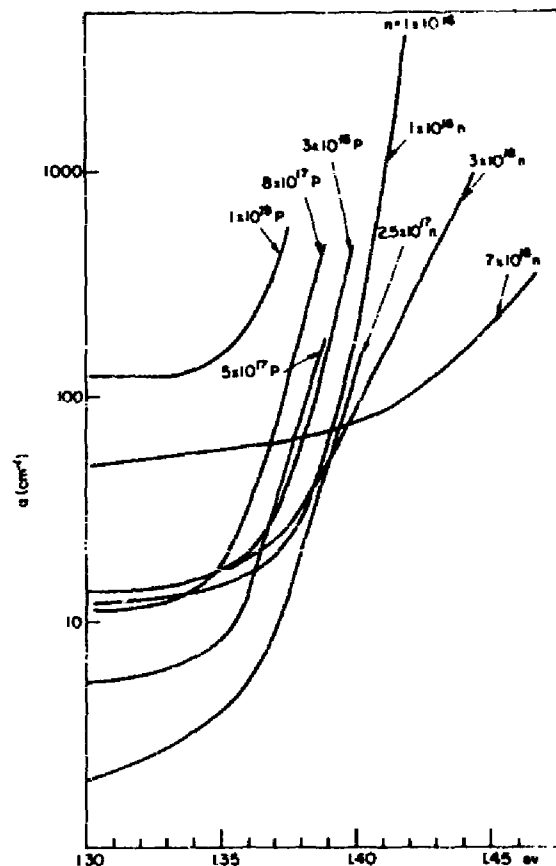


Fig. 2. Room-temperature absorption spectra of seven differently doped specimens of GaAs. (Specimen  $P = 5 \times 10^{17}$  is doped with zinc and is partly compensated with about  $10^{17}$  tin atoms/cm<sup>3</sup>.)

somewhat larger) we did not see any structure in the absorption edge which might have suggested a transition to a donor state. The shift of the absorption edge to lower energy was also seen in a single specimen of GaAs after a copper diffusion treatment which converted the material to  $p$ -type conductivity. Low temperature measurements are underway for a more precise determination of the band edge in  $n$ -type material where, because of the low density of state effective mass, the filling of the conduction band must be carefully taken into account.

We are grateful to D. A. Kramer and J. E. Berkeyheiser for their assistance in these measurements and to F. Hawrylo for his assistance in the fabrication of the diodes.

<sup>1</sup>M. I. Nathan and G. Burns, *Appl. Phys. Letters* 1, 89 (1962).

<sup>2</sup>J. I. Pankove, *Phys. Rev. Letters* 9, 283 (1962).

<sup>3</sup>D. F. Nelson, M. Gershenzon, A. Ashkin, L. A. D'Asaro, and J. C. Sarace, *Appl. Phys. Letters* 2, 182 (1963).

<sup>4</sup>L. J. Vieland and I. Kudman, *J. Phys. Chem. Solids* 24, 437 (1963).

<sup>5</sup>M. D. Sturge, *Phys. Rev.* 127, 1559 (1962).

<sup>6</sup>M. I. Nathan and G. Burns, *Phys. Rev.* 129, 125 (1963).

<sup>7</sup>C. Haas, *Phys. Rev.* 125, 1965 (1962).

<sup>8</sup>J. I. Pankove and P. Aigrain, *Phys. Rev.* 126, 756 (1962).

<sup>9</sup>I. Kudman and L. J. Vieland, *J. Phys. Chem. Solids* (to be published).

**UNCLASSIFIED**

**UNCLASSIFIED**